

Indirect Quantum Control: An Implementation-Independent Scheme

by

David Layden

A thesis
presented to the University of Waterloo
in fulfillment of the
thesis requirement for the degree of
Master of Mathematics
in
Applied Mathematics (Quantum Information)

Waterloo, Ontario, Canada, 2016

© David Layden 2016

This thesis consists of material all of which I authored or co-authored: see Statement of Contributions included in the thesis. This is a true copy of the thesis, including any required final revisions, as accepted by my examiners.

I understand that my thesis may be made electronically available to the public.

Statement of Contributions

Parts of this thesis have been adapted from Refs. [64, 65, 40], which I authored or co-authored. In particular, Chapters 3 and 4 are based on [64] and [65] respectively, of which I am the lead author. I performed all of the calculations and computations contained in both of these works, and contributed significantly to their writing. Chapter 5 is based in part on [40], of which I am a co-author and Daniel Grimmer, currently a Master's student at the University of Waterloo, is the lead author. The material presented in this chapter, however, represents only a subset of that in [40], and contains solely my own work (although some of the results in Chapter 5 were discovered independently by Daniel).

Abstract

The ability to control quantum systems rapidly as compared to their coherence times is a central requirement for most proposed quantum technologies, such as quantum computing and quantum metrology. Improving the ratio of control timescales to coherence times, however, is made difficult by the fact that both timescales depend on the coupling strength between systems and their environment. One promising method of improving this ratio involves indirect control: steering a quantum system via a quantum actuator, rather than by driving it directly. While this approach has shown promise in a variety of experimental settings, all implementations to date have relied crucially on special properties of the system at hand, and the control schemes they have used are not generally applicable to arbitrary systems.

Here we propose an implementation-independent indirect control scheme. It relies upon an unexpected emergent feature of a model in which a quantum system is made to interact with a rapid succession of ancillas, one at a time. We introduce this model by discussing the quantum Zeno effect, a special instance of quantum control in which a state is preserved through frequent measurements. We then further develop the model and show how it can be used to construct a universal scheme for indirect quantum control. Finally, we discuss the possibility of using this scheme not only for coherent control, but also for dissipative quantum control, which has a number of important applications.

Acknowledgements

First and foremost, I wish to thank my supervisor Prof. Achim Kempf for his guidance, his tireless support, and for his exceptional ability to gauge the academic needs of his students. I also wish to thank Prof. Eduardo Martín-Martínez for all of the precious time and effort he dedicated to these projects. I would also like to thank Prof. Raymond Laflamme and Prof. Lorenza Viola for valuable discussions, as well as Prof. Robert Mann for his involvement in some of this work.

I wish to thank my friends and colleagues Paulina Corona-Ugalde, Daniel Grimmer, Robert Jonsson, Mikhail Panine, Jason Pye, Nayeli Rodríguez-Briones, and Guillaume Verdon-Akzam for countless relevant discussions, and for just as many less relevant—but equally interesting—ones.

Finally, I wish to thank my parents and my partner Sarah, without whom none of this would have been possible.

Table of Contents

List of Tables	ix
List of Figures	x
1 Introduction	1
2 Background	3
2.1 Open Quantum Systems	3
2.2 Quantum Control	6
2.3 Repeated Interaction Systems	8
3 Finite Frequency Quantum Zeno Effect	10
3.1 Motivation	10
3.2 Setting	15
3.3 A Qubit Model	17
3.3.1 Recovering the conventional quantum Zeno effect as a special case .	17
3.3.2 Realistic settings	19
3.4 The System-Detector Interaction as a Measurement	23
3.4.1 An idealized example	24
3.4.2 A realistic example	24
3.5 Discussion	25

4	Indirect Quantum Control: Coherent Control	27
4.1	Motivation	27
4.1.1	An existing indirect control scheme	30
4.2	The Scheme	31
4.2.1	Mathematical intuition	33
4.3	Main Result	33
4.3.1	Relation to the quantum Zeno effect	37
4.3.2	Interpretation	38
4.3.3	An example	38
4.4	Error Analysis	40
4.4.1	Truncation error	41
4.4.2	Stroboscopic error	44
4.5	Discussion	45
5	Indirect Quantum Control: Dissipative Control	48
5.1	Motivation	48
5.2	An Effective System Liouvillian	49
5.3	Higher-Order Propagators	52
5.3.1	Numerical test	53
5.4	Stroboscopic Error at Higher Orders	54
5.5	Discussion	58
6	Conclusions	60
	APPENDICES	62
A	Eigenpairs of the channel Φ	63

B	Applying Chernoff's Theorem	65
B.1	Continuity of $\Phi(\delta t)$	66
B.2	Linearity and contractivity of $\Phi(\delta t)$	67
B.3	$\Phi(0)$ is the identity operator on B	68
B.4	Existence of $\Phi'(0)$ and semigroup property	68
C	Simulation Details	70
	References	72

List of Tables

2.1	Typical Control Timescales and Coherence Times	8
3.1	Eigenpairs describing a conventional quantum Zeno effect	14
3.2	Eigenpairs describing the qubit model in the high frequency limit	18

List of Figures

3.1	Fixed points of Φ	22
4.1	Schematics of direct and indirect control	29
4.2	Schematic of actuator reinitialization	36
4.3	Fidelity in implementing H_{eff}	40
C.1	Convergence of simulation in truncated Hilbert space	71

Chapter 1

Introduction

In recent decades, quantum mechanics has evolved beyond its original role as a description of nature, into a platform underlying a number of emerging technologies. This evolution has occurred due to two complementary developments: On one hand, spectacular experimental advances since the early days of quantum physics have enabled not only the direct observation, but also the control of manifestly quantum systems. On the other hand, theoretical advances have revealed a number of potential applications for controllable quantum devices, which are collectively termed *quantum technologies*. For many quantum technologies, such as quantum computing and quantum simulation, the difference in performance between quantum devices and their classical counterparts becomes important primarily when the former are sufficiently complex, and can no longer be simulated classically.

Correspondingly, one of the main ingredients required to develop such quantum technologies is the ability to accurately steer complex quantum systems. This task is greatly complicated, however, by the fact that quantum systems invariably experience decoherence: Realistic quantum systems are open—that is, they are coupled to their environment, and are consequently affected by it in random and largely uncontrollable ways. Unlike in classical systems however, this jostling from the environment can cause quantum systems not only to gain/lose energy, but also to acquire phase uncertainty, gradually robbing them of their distinctly quantum nature [115, 116]. Understandably, most proposed implementations of quantum technologies seek to suppress the effects of decoherence in some manner.

There exist a number of techniques for reducing the effects of decoherence. Perhaps most notable among them is quantum error correction [91, 94, 67], although other approaches such as dynamical decoupling [101, 100, 102, 11] or the use of decoherence free

subspaces [66, 62, 56] (which may be used in tandem with error correction) can also be highly effective. Error correcting codes operate on the level of quantum “software”, as opposed to hardware. On the hardware level, however, the most immediate way of taming decoherence is by striving to control quantum systems rapidly as compared to their coherence times. This can be achieved by improving systems’ coherence times, or, in the case of the present work, by controlling quantum systems more rapidly. An improvement in the ratio of control timescales to coherence times on the hardware level is, in turn, a boon to software-level techniques such as error correction. In the language of quantum computing, for instance, improving this ratio reduces the number of errors per gate, which reduces the overhead required for quantum error correction [59].

This thesis presents a novel method for improving the ratio of control timescales to coherence times of quantum systems using “indirect quantum control”. Rather than driving a quantum system directly (an approach we will term “direct quantum control”), indirect control seeks to steer a target system by driving an auxiliary quantum system to which the target is coupled. The thesis is organized as follows: Chapter 2 reviews the requisite preliminaries, and Chapter 3 introduces the model underlying our scheme by briefly applying it to the quantum Zeno effect, along the lines of [64]. Using the formalism developed through this tangential application, Chapter 4 presents the novel indirect control technique from [65], and Chapter 5 explores various extensions thereof, and in doing so, introduces a number of technical tools from [40].

Chapter 2

Background

In this chapter we briefly review the background material for this thesis.

2.1 Open Quantum Systems

We will mostly use density operators, as opposed to “kets”, throughout this thesis to describe quantum states. If \mathcal{H} is the Hilbert space associated with a quantum system, the system’s state can be described by a linear operator $\rho : \mathcal{H} \rightarrow \mathcal{H}$, such that the expectation value of an observable X with respect to the state is given by $\langle X \rangle = \text{tr}(X\rho)$. To ensure a physically reasonable description of the system’s state, we require that (i) ρ be self-adjoint, (ii) $\rho \geq 0$, and (iii) $\text{tr}(\rho) = 1$. A key feature of this formalism is that it encompasses both pure and mixed states, which is essential for describing realistic experimental settings.

A useful tool when employing density operators is that of a *superoperator*: an operator which maps the set of operators on \mathcal{H} to itself. (A more formal discussion of the various sets and spaces involved here can be found in Appendix B.) A particularly important type of superoperator is a completely positive trace-preserving (CPTP) map, also known as a *quantum channel* [80]. Quantum channels are of special interest because they map density operators to density operators. This important feature makes quantum channels the density operator-analogues of unitaries on \mathcal{H} , which map normalized kets to normalized kets. Building upon this analogy, in the same way that a family of unitaries $\{U(t)\}$ on \mathcal{H} can encode the time evolution of a ket, a family of quantum channels can do so for density operators. Concretely, just as we have $|\psi(t)\rangle = U(t)|\psi(0)\rangle$ for kets, we may also have $\rho(t) = \Phi(t)\rho(0)$ for density operators, for some quantum channel $\Phi(t)$. In this context, $\Phi(t)$ is sometimes known as a *dynamical map*.

The analogue of the Schrödinger equation for density operators is the *von Neumann equation*:

$$\frac{d\rho}{dt} = -\frac{i}{\hbar}[H, \rho], \quad (2.1)$$

where H is the system's Hamiltonian (which may be time-dependent in general). Eq. (2.1) can be expressed more compactly by defining the *Liouvillian superoperator*, or simply *Liouvillian*, $\mathcal{L} \cdot = -\frac{i}{\hbar}[H, \cdot]$. One can then write the von Neumann equation in terms of \mathcal{L} as

$$\frac{d\rho}{dt} = \mathcal{L}\rho, \quad (2.2)$$

where any time dependence in H will result in a correspondingly time-dependent \mathcal{L} . Notice that the Liouvillian \mathcal{L} plays an analogous role for density operators as the Hamiltonian does for kets: it serves as the generator of time translations. Moreover, just as the solution of the Schrödinger equation with a time-independent H is $|\psi(t)\rangle = \exp(-iHt/\hbar)|\psi(0)\rangle$, the solution of the von Neumann equation in the same case is $\rho(t) = \exp(\mathcal{L}t)\rho(0)$, which can be expanded into the form

$$\rho(t) = e^{-iHt/\hbar}\rho(0)e^{iHt/\hbar}, \quad (2.3)$$

as one would expect. More generally, and analogously to the Schrödinger equation, the general solution to the von Neumann equation with a time-dependent H (and therefore a time-dependent \mathcal{L}) can be expressed using a time-ordered exponential:

$$\rho(t) = \mathcal{T} \exp \left[\int_0^t d\tau \mathcal{L}(\tau) \right] \rho(0). \quad (2.4)$$

Note that while \mathcal{L} is a superoperator it is not a quantum channel since it is not CPTP, so it does not map density operators to density operators. The exponential of \mathcal{L} (time-ordered and integrated as needed), however, is a quantum channel and a dynamical map.

The von Neumann equation, like the Schrödinger equation, describes a purely unitary system dynamics. However, realistic quantum systems seldom evolve unitarily. The reason for this non-unitarity is that quantum systems are typically coupled to an environment. While the combined system-environment object may evolve unitarily, environmental degrees of freedom cannot be directly observed, and so they are averaged over (through a partial trace) to yield an effective reduced dynamics for the system. This reduced dynamics is usually non-unitary due to entanglement between the system and the environment that generically arises due to coupling between the two.

Providing an exact description of a system's open dynamics is often exceedingly difficult. In principle, such a description can be arrived at by solving for the overall system-environment dynamics and then tracing over environmental degrees of freedom. However, the nature of the environment (specifically, its state and free dynamics) is inevitably unknown, as is the form of the system-environment coupling. An effective description of the system's dynamics is therefore needed.

There exist numerous ways of describing open quantum dynamics, ranging from stochastic differential equations modelling noise [38] to integro-differential equations which encode the environment's action on the system through a convolution term in the generator of the system's reduced dynamics [13]. Throughout this thesis, however, it will suffice to use a simpler—albeit ubiquitous—description of open quantum dynamics: the Lindblad equation [68].

The Lindblad equation can be derived by first noting that $\mathcal{L} \cdot = -\frac{i}{\hbar}[H, \cdot]$ is not the most general Liouvillian which guarantees that the solution of $\frac{d\rho}{dt} = \mathcal{L}\rho$ be a family of valid density operators. In fact, this requirement is satisfied by any equation of the form

$$\frac{d\rho}{dt} = \underbrace{-\frac{i}{\hbar}[H, \rho] + \sum_{j,k} c_{jk} \left[L_j \rho L_k - \frac{1}{2} \{ \rho, L_k^\dagger L_j \} \right]}_{\mathcal{L}\rho}, \quad (2.5)$$

where $\{L_j\}$ are operators on the system's Hilbert space, and where the matrix $C = (c_{jk})_{j,k}$ is positive. (Note that braces are used to denote an anti-commutator in the equation above.) Eq. (2.5) can be simplified by diagonalizing C . In particular, since $C > 0$, there exists a unitary matrix U which diagonalizes C [i.e., there is a unitary U such that $U^\dagger C U = \text{diag}(\lambda_1, \dots, \lambda_n) > 0$]. Defining operators $A_k = \sum_j u_{jk} L_j$, where u_{jk} is the jk -th element of U , the Liouvillian in (2.5) can be rewritten as [13]

$$\mathcal{L}\rho = \underbrace{-\frac{i}{\hbar}[H, \rho] + \sum_j \lambda_j \left[A_j \rho A_j - \frac{1}{2} \{ \rho, A_j^\dagger A_j \} \right]}_{\mathcal{D}\rho}, \quad (2.6)$$

where we have defined the dissipation superoperator, or dissipator, \mathcal{D} , such that $\mathcal{L} = -\frac{i}{\hbar}[H, \cdot] + \mathcal{D}$. Note that the $-\frac{i}{\hbar}[H, \cdot]$ term here is known as the Hamiltonian part of \mathcal{L} .

The Lindblad equation follows from the approximation that the environment dissipates information about the system's state instantaneously and irreversibly (much like a thermal bath). In other words, it assumes that information about the system at a time t_1 cannot be temporarily encoded in the environment only to affect the environment's impact on

the system at a later time t_2 . This feature is known as Markovianity, and the Lindblad equation is the most general possible Markovian equation of motion for the system. Thus, the Lindblad equation describes only a special case of open quantum dynamics. However, it often provides an excellent phenomenological descriptions of real systems, given the right choice of operators $\{A_j\}$.

2.2 Quantum Control

Quantum control is a field concerned with the purposeful steering of quantum systems. It typically involves preparing a particular state of a quantum system, or, performing a desired operation on a quantum system. This thesis will be chiefly concerned with the latter objective, although we will at times touch on the former as well. Quantum control came into prominence several decades ago in the field of quantum chemistry, where researchers sought to steer chemical reactions towards desired outcomes (which may not occur naturally) by subjecting reagents to carefully shaped and timed laser pulses [90]. More recent applications of quantum mechanics, however, such as quantum metrology, simulation, and computing, also require accurate and non-trivial steering of quantum systems. Today, quantum control represents an essential ingredient for most proposed quantum technologies.

In terms of the formalism introduced in the previous section, the general problem of quantum control is that of finding a time-dependent Liouvillian $\mathcal{L}(t)$ which has the effect of implementing some specific quantum channel on a system over a time interval $[0, t]$. In particular, we will largely be concerned here with implementing channels corresponding to unitary operations (modulo decoherence). This general problem is made more specific through two constraints often imposed by experiments:

1. In most experimental settings one does not have direct control over the dissipative part of the system's dynamics (although we will discuss an exception in Chapter 5). Moreover, realistic dissipation processes are usually described by a time-independent dissipator \mathcal{D} , determined by the experimental setup at hand. Thus, quantum control problems often do not involve finding a general Liouvillian $\mathcal{L}(t)$ which produces a desired channel, but rather, a Hamiltonian $H(t)$ which does so, where

$$\mathcal{L}(t) = -\frac{i}{\hbar}[H(t), \cdot] + \mathcal{D} \tag{2.7}$$

for some given \mathcal{D} .

2. In practice, one typically has access to only a limited family of time-dependent Hamiltonians $H(t)$, as determined by the experimental setup. The usual structure of this Hamiltonian is

$$H(t) = H_0 + H_c(t). \quad (2.8)$$

Here, H_0 is the system's free Hamiltonian and $H_c(t)$ is known as the control Hamiltonian. This structure arises because quantum systems are often controlled by being subjected to a classical electromagnetic (EM) field, which an experimenter can modify. The form of $H_c(t)$, then, depends on how the system couples to this EM field. Eq. (2.8) arises in numerous physical systems, such as nuclear magnetic resonance (NMR) and electron spin resonance (ESR) setups, as well as in superconducting qubits and trapped ions, where experimentalists can implement a specific $H_c(t)$ by applying a carefully shaped EM pulse to the system. Naturally, limitations on the kind of pulses that can be generated in a particular experiment pose further constraints on $H_c(t)$ [46].

Adapting techniques from classical control theory, Lloyd showed in Ref. [69] that an appropriate choice of $H_c(t)$ can produce any desired unitary operation U on the system. (This is true at least for closed finite-dimensional systems, provided the algebra generated by H_0 and $H_c(t)$ through commutation includes all Hamiltonians for the system, which is almost always the case [69].) A variety of techniques have been developed for finding $H_c(t)$ that will produce a given U , provided there exists such an $H_c(t)$. For example, Gradient Ascent Pulse Engineering (GRAPE) [57] is a widely-used numerical technique addressing this problem, which progressively refines an ansatz for $H_c(t)$ by minimizing the discrepancy between its effect on the system and that of U . Such techniques have proved highly effective for simple systems. However, they tend to scale poorly to more complex ones due to, among other reasons, the rapid growth in computational cost with increased system complexity [81]. Therefore, methods of reducing the complexity involved in finding $H_c(t)$ for high-dimensional quantum systems have the potential to be very useful.

The above discussion has been primarily concerned with implementing unitary operations on a system. Efforts to do so, however, are obviously hampered by dissipation, which is generally present in the dynamics of real quantum systems. While there exist methods of effectively suppressing dissipation (via dynamical decoupling for instance [101, 100, 102, 11]), the simplest, and perhaps the most common strategy, is to perform control operations quickly as compared to the timescale of \mathcal{D} . Unfortunately, the speed with which a system can be directly controlled and the rate at which it experiences decoherence are related. In particular, both timescales depend similarly on the coupling strength between the system and its environment. A system strongly coupled to its environment

(i.e., with a system-environment coupling frequency that is large compared to the system’s free dynamics) will be strongly impacted by it, and will typically have shorter coherence times as a result. (The opposite is true for weak system-environment couplings.) On the other hand, rapid control of a system requires $\|H_c(t)\|$ to take on large values. For many experiments this means that the system must couple strongly to the classical EM field used to control it, which is part of the environment. Therefore, rapid control tends to come with short coherence times, and conversely, long coherence times tend to come with slower control. This broad trend can be seen by comparing the coherence times and gate times of various implementations of quantum information processing: while these can vary by many orders of magnitude depending on the physical system at hand, the ratio between control and decoherence timescales varies significantly less (see Table 2.1).

System	Gate Time	Coherence Time	# Gates / Coherence Time
Superconducting Qubits [8]	10–20 ns	20–40 μ s	1 000–4 000
NV Centres [1]	1–10 μ s	5–10 ms	500–10 000
Trapped Ions [49]	\sim 100 μ s	\sim 1 s	\sim 10 000

Table 2.1: Typical control timescales (specifically, gate times) and typical coherence times for various quantum systems. Notice, for different systems, that while both of these timescales vary by many orders of magnitude, their ratio (specifically, the number of gates per coherence time) shows little variation.

2.3 Repeated Interaction Systems

Subsequent chapters in this thesis will use a model known as a *Repeated interaction system* (RIS), also called a *collision model*. It is based on a simple premise: a quantum system S is coupled to an ancilla A_1 (with which it is initially uncorrelated) and the pair is allowed to evolve together for some period of time. Then, A_1 is discarded, and the system is coupled to a new ancilla A_2 , and so on. We will refer to the interval between subsequent ancillas being discarded as a cycle. The usual goal when studying RIS models is to determine the effect on the system of a series of such cycles.

In the present work we will take all the ancillas to be of the same type. That is, we will assume their Hilbert spaces to be of the same dimension and their free dynamics to be identical. Moreover, we will take them to couple identically to the system, and we will

usually consider cycles of uniform duration. We will focus initially on the case where the initial state of every ancilla (when each is first coupled to S) is identical, and we will denote this state as ρ_A .

Repeated interaction systems have been studied for a variety of purposes in recent years. In particular, Refs. [6, 5, 4, 99, 39] examine the mathematical underpinnings of these models, Refs. [87, 112, 113, 114] use them to gain insight into the processes of thermalization and decoherence, and Refs. [19, 17, 20, 55, 18, 21, 43] use them as a tool to study quantum thermodynamics. The main application of RIS models in this thesis is as a tool for quantum control, as presented in Chapters 4 and 5. In order to lead into these chapters, however, we first consider a tangential application of repeated interaction systems: that of describing the quantum Zeno effect. (This effect could be seen as a special instance of quantum control, concerned with state preservation instead of general steering.) Chapter 3 presents a self-contained study of how an RIS model can describe the Zeno effect in a manner that does away with many of the usual idealizations. This brief study will serve to introduce the formalism used in Chapters 4 and 5.

Chapter 3

Finite Frequency Quantum Zeno Effect

In this chapter we present the material published in [64]. While the mathematics underlying these results is very similar to that used in later chapters, the physics is rather different (and only somewhat related to quantum control). As a result, this chapter is meant to be mostly self-contained, and to serve as an example-based introduction to formalism that will be used more abstractly in subsequent chapters.

3.1 Motivation

The quantum Zeno effect (QZE) is a phenomenon whereby frequent identical measurements of a quantum system inhibit its evolution. In the limit of infinitely frequent measurements, the system can become frozen entirely. If the measurements are projective, a system prepared in a measurement eigenstate, or in an incoherent mixture of measurement eigenstates, will have its evolution halted in the high measurement frequency limit¹.

Suppose, for illustration, that a closed system evolves according to a time-independent Hamiltonian H , and that n projective measurements described by an operator M are performed at uniform intervals within a time t . Moreover, suppose that the system is

¹If the measurement operator has a degenerate spectrum, i.e., if two or more orthogonal eigenstates can correspond to the same measurement outcome, then the situation is more complex. In particular, the system's state can become trapped in such a multi-dimensional subspace and evolve non-trivially within it in the high frequency limit, see e.g., [32]. We will not be directly concerned with this possibility here.

initially prepared in the state $|\psi\rangle$, an eigenstate of M belonging to a one-dimensional measurement eigenspace. The probability that the first measurement, performed at a time t/n , finds the system to be in the state $|\psi\rangle$ is given by

$$P_{\text{surv}}(t/n) = \left| \langle \psi | e^{-iHt/n\hbar} | \psi \rangle \right|^2, \quad (3.1)$$

which we call the *survival probability* for a time t/n . The propagator in the equation above can be expanded in powers of $1/n$ as

$$e^{-iHt/n\hbar} = I - \frac{iHt}{n\hbar} - \frac{H^2 t^2}{2n^2 \hbar^2} + \mathcal{O}(1/n^3). \quad (3.2)$$

Substituting this expansion into (3.1) and collecting powers of n yields

$$P_{\text{surv}}(t/n) = 1 - \frac{t^2}{n^2 \hbar^2} \underbrace{\left(\langle H^2 \rangle - \langle H \rangle^2 \right)}_{\Delta H^2} + \mathcal{O}(1/n^3). \quad (3.3)$$

The probability that the system be found in the state $|\psi\rangle$ in both the first and the second measurement is then given by $P_{\text{surv}}(2t/n) = P_{\text{surv}}(t/n)^2$, and more generally, the probability that it be found in the state $|\psi\rangle$ for all n measurements is given by

$$\begin{aligned} P_{\text{surv}}(t) &= P_{\text{surv}}(t/n)^n \\ &= \left[1 - \frac{t^2 \Delta H^2}{n^2 \hbar^2} + \mathcal{O}(1/n^3) \right]^n \\ &= 1 - \frac{t^2 \Delta H^2}{n \hbar^2} + \mathcal{O}(1/n^2) \rightarrow 1 \text{ as } n \rightarrow \infty. \end{aligned} \quad (3.4)$$

Thus, as the number of measurements performed within a fixed time interval increases, the probability of finding the initial state to be unchanged in all of the measurements approaches unity. In other words, the system's dynamics is inhibited at high measurement frequencies and frozen altogether in the high frequency limit. It follows immediately that the same effect occurs if the system is initially prepared in an incoherent combination of measurement eigenstates. For instance, a qubit undergoing repeated σ_x measurements will have all states along the x -axis of the Bloch sphere [that is, all states of the form $\rho = \frac{1}{2}(I + \epsilon\sigma_x)$] frozen as the measurement frequency tends to infinity.

The QZE sharply contrasts the nature of measurements in quantum physics with that in classical physics. However it also promises a number of applications, notably in quantum

information processing, where it is been proposed as a tool for quantum error correction [31, 82, 30], state preparation [78, 79, 105], gate implementation [35], and for confining systems to decoherence-free subspaces [9].

Notice two idealizations in the calculation above which are typical when describing the quantum Zeno effect:

1. The measurements were assumed to be perfect, in that they were projective in nature and occurred instantaneously.
2. The state of the system is only entirely frozen in the unphysical limit of infinite measurement frequency.

In this chapter we introduce mathematical tools (which we will expand upon in Chapters 4 and 5) to analyse an RIS model that will provide a description of the QZE which does not invoke these idealizations. Perhaps surprisingly, we will find that imperfect measurements can enable perfect freezing of quantum systems when they are repeated at special finite frequencies. The usual high frequency limit is but one of these special frequencies.

We begin by examining closely the role of measurement in the QZE with the help of a simple example.

Example 3.1. Consider a qubit which evolves unitarily under the Hamiltonian $H = \hbar\omega\sigma_z$, and which undergoes periodic projective σ_x measurements. As per the discussion above, all initial qubit states of the form $\rho = \frac{1}{2}(I + \epsilon\sigma_x)$ will become frozen as the measurement frequency tends to infinity.

Suppose, in contrast with the previous calculation, that the measurement results are not known to the experimenter. In this case, the effect of each measurement on the qubit is

$$\rho \mapsto \mathcal{M}\rho := \left(\langle +|\rho|+ \rangle \cdot |+\rangle\langle +| \right) + \left(\langle -|\rho|- \rangle \cdot |-\rangle\langle -| \right), \quad (3.5)$$

where $|\pm\rangle = \frac{1}{\sqrt{2}}(|0\rangle \pm |1\rangle)$, and where we have defined the superoperator \mathcal{M} to describe the effect of a “blind” measurement. Eq. (3.5) describes a process in which a pre-measurement state ρ is projected to the state $|+\rangle\langle +|$ with probability $\langle +|\rho|+ \rangle$, and to the state $|-\rangle\langle -|$ with probability $\langle -|\rho|- \rangle$. Without knowing the result of the measurement, we must describe the post-measurement state as an incoherent combination of the two possible outcomes.

As a technical tool, we also define the dynamical map $\mathcal{U}(t/n)$ as

$$\mathcal{U}(t/n)\rho := e^{-iHt/n\hbar}\rho e^{iHt/n\hbar}, \quad (3.6)$$

which describes free evolution of the system for a time t/n between successive measurements. The effect on the qubit of one evolve-and-measure cycle of duration t/n , then, is given by the channel $\Phi(t/n) := \mathcal{M} \circ \mathcal{U}(t/n)$. The eigenpairs $\{V_j(n), \lambda_j(n)\}$ of $\Phi(t/n)$, found by inspection, are shown in Table 3.1.

While $V_1(n), \dots, V_4(n)$ are matrices, they are eigenvectors of $\Phi(t/n)$ (a linear operator) in the sense that $\Phi(t/n)V_j(n) = \lambda_j(n)V_j(n)$. Note that we are treating $t > 0$ as a fixed constant here and n , the number of measurements made in the interval $[0, t]$, as a variable. Observe that $\{V_j(n)\}$ forms a basis for 2×2 Hermitian matrices² for all $n > 0$; this implies that for any n there exist coefficients $c_j(n)$ such that any initial system state $\rho(0)$ can be decomposed as $\rho(0) = \sum_j c_j(n)V_j(n)$. This representation of $\rho(0)$ is convenient as it allows us to easily characterize the high measurement frequency limit. In particular, the state of the system after performing n evenly-spaced measurements in a time t is given by

$$\begin{aligned} \rho(t) &= \Phi(t/n)^n \rho(0) \\ &= \Phi(t/n)^n \sum_{j=0}^3 c_j(n)V_j(n) \\ &= \sum_{j=0}^3 c_j(n)\Phi(t/n)^n V_j(n) \\ &= \sum_{j=0}^3 c_j(n)\lambda_j(n)^n V_j(n). \end{aligned} \quad (3.7)$$

Note that since the basis $\{V_j(n)\}$ changes with n , so too must the coordinates $c_j(n)$ used to describe a fixed initial state $\rho(0)$ in this basis.

Taking $n \rightarrow \infty$ in the previous expression (referring to Table 3.1), one immediately finds that as the measurement frequency goes to infinity, the state of the system at a time t is given by

$$\rho(t) = \frac{1}{2} \left(I + \langle \sigma_x \rangle_0 \sigma_x \right), \quad (3.8)$$

²The matrices $\{V_j(n)\}$ form a basis for $\text{herm}(2)$ except at isolated values of t where $\cos(2\omega t/n) = 0$. This will not be an issue for us as we will consider the large n limit.

where $\langle \sigma_x \rangle_0 := \text{tr}[\rho(0)\sigma_x]$ is the σ_x component of the system's initial state. In other words, initial states of the form $\rho(0) = \frac{1}{2}(I + \epsilon\sigma_x)$ will be frozen in the high measurement frequency limit even though the measurement outcomes are not known to the experimenter.

Eigenvalues	Eigenvectors
$\lambda_0(n) = 1$	$V_0(n) = I$
$\lambda_1(n) = \cos(2\omega t/n)$	$V_1(n) = \sigma_x$
$\lambda_2(n) = 0$	$V_2(n) = \sin(2\omega t/n)\sigma_x + \cos(2\omega t/n)\sigma_y$
$\lambda_3(n) = 0$	$V_3(n) = \sigma_z$

Table 3.1: Eigenvalues and eigenvectors of the channel $\Phi(t/n)$ which describes evolution by $H = \hbar\omega\sigma_z$ for a time t/n followed by a projective σ_x measurement whose result is not known.

The result of Example 3.1 is not surprising: we could have anticipated it simply from the fact that the Zeno effect does not involve feedback. That is, the result of a measurement performed at time t_1 is not used to impact the system at a later time t_2 . Thus, whether or not the measurement results are known is of no consequence to the physics at hand. This is a crucial point, and it is true in general: *The quantum Zeno effect arises due to measurement back-action*. What matters is only that identical measurements be repeated at a high frequency—their outcomes are largely irrelevant.

With this observation in mind, and with the goal of eliminating the idealizations of perfect measurements performed at infinite frequency, we will examine the quantum Zeno effect using a different description of measurement. In particular, we will raise the Heisenberg cut: the imaginary (and in principle, movable) division between a system that is treated quantum mechanically and the rest of the world, which is treated classically. In particular, we will adopt a quantum-mechanical description of the measurement device(s)—which we will refer to as the *detector(s)*—performing the repeated measurements. Such a description will not invoke the typical measurement postulate or any form of wavefunction collapse, as it will be purely dynamical. We will see that the back-action on the system due to an interaction with a quantized detector will lead to a rich variety of Zeno-like phenomena—including, as a special case, the conventional QZE—which need not invoke the idealizations of perfect measurements performed at an infinite frequency.

3.2 Setting

We will model the repeated measurements underlying the QZE with a system S which is periodically made to interact with a succession of quantum-mechanical detectors, each of which we denote as D . To ensure that the effect of each measurement on the system is identical, as in the traditional Zeno scenario, we will assume all of the detectors to have the same free dynamics and to be prepared in the same initial state ρ_D . Moreover, for simplicity, we will take the aggregate dynamics of the system and detectors to be unitary—an assumption we will relax in later chapters.

Concretely, we suppose the system S is initially prepared in the state $\rho_S(0)$, and that it evolves under its free Hamiltonian H_S for a time interval δt_F (“ F ” for “free”). It is then coupled to a detector D prepared in the state ρ_D , and the pair evolves together for a period δt_M (“ M ” for “measurement”) according to the *measurement Hamiltonian* $H_M = H_S + H_D + H_{SD}$, where H_{SD} describes the system-detector coupling. (We take all Hamiltonians here to be time independent, although we will allow time dependence in subsequent chapters.) This interaction constitutes a measurement in the sense that information about the system’s state becomes encoded in the detector through their interaction. After the measurement has taken place, S and D are uncoupled and the cycle begins anew, using either a fresh detector every time, or resetting the same one to the state ρ_D before re-coupling it to the system. Notice that this constitutes an RIS model where the ancillas play the role of quantum-mechanical detectors (which is why we denote them here as D rather than A).

As in Example 3.1, we will describe the net effect of each evolve-and-measure cycle on the system through a dynamical map Φ , defined here as

$$\Phi\rho_S := \text{tr}_D \left\{ e^{-iH_M \delta t_M/\hbar} \left[\left(e^{-iH_S \delta t_F/\hbar} \rho_S e^{iH_S \delta t_F/\hbar} \right) \otimes \rho_D \right] e^{iH_M \delta t_M/\hbar} \right\}. \quad (3.9)$$

(We will not explicitly write the functional dependence of Φ , say on δt_F and δt_M , as doing so would lead to cumbersome notation as we introduce more parameters into our model.) The effect of many cycles on S can be described by repeated applications of Φ . Concretely, a system initially prepared in the state $\rho_S(0)$ will be mapped to the state $\Phi^n \rho_S(0)$ after n cycles, where

$$\Phi^n \rho_S(0) = \underbrace{\Phi \circ \Phi \circ \dots \circ \Phi}_{n \text{ times}} \rho_S(0). \quad (3.10)$$

In order to describe the effect of many cycles on S , we will aim to find the eigenvectors and eigenvalues of the channel Φ as functions of δt_F , δt_M , and other parameters which

we will soon introduce. That is, as in Example 3.1, we wish to find linear operators $\{V_j\}$ on the system’s Hilbert space, and complex numbers $\{\lambda_j\}$, such that $\Phi V_j = \lambda_j V_j$. We note that, as in the previous example, these eigenvectors need not correspond to density matrices when considered alone—however, they generically form a basis³ in which we will express the initial system state as $\rho_S(0) = \sum_j c_j V_j$. As in Example 3.1, the system’s state after n cycles will be given by

$$\rho_S(n \delta t) = \sum_j c_j \lambda_j^n V_j, \quad (3.11)$$

where we denote the total cycle duration as $\delta t := \delta t_F + \delta t_M$.

An immediate consequence of Eq. (3.11) is that the system’s fate after many cycles depends on its initial state (specifically, on $\{c_j\}$) and on the spectrum of Φ . Since the map Φ is CPTP, its eigenvalues all lie within the closed unit disk centred about the origin of the complex plane [106]. Thus, components of $\rho_S(0)$ belonging to eigenspaces with $\lambda = 1$ will be preserved by repeated applications of the channel, those in eigenspaces with $|\lambda| < 1$ will be exponentially suppressed, and those in eigenspaces with $|\lambda| = 1$ but $\lambda \neq 1$ will not decay with growing n , but rather, will acquire a complex phase⁴.

The fact that Φ is CPTP has an implication that will be of paramount importance in this chapter: there always exists *at least one* system state ρ_S which is a fixed point of Φ , and is therefore exactly preserved by the evolve-and-measure cycles [80]. That is, regardless of the Hamiltonians involved, the initial state of the detectors, the duration of the cycles etc., there always exists a system state such that $\Phi \rho_S = \rho_S$, and therefore $\Phi^n \rho_S = \rho_S$ for all integer n . This fact is a direct consequence of a result from functional analysis called Brouwer’s fixed point theorem [16]. Notice that in Example 3.1 the maximally mixed state was a fixed point of the channel, although we will see that this “Brouwer fixed point” can, in general, be anywhere in the system’s state space.

Fixed points of Φ belong to eigenspaces with $\lambda = 1$. There is also a related possibility that would produce similar physics: A system state that has components in eigenspaces with $\lambda \approx 1$ can be almost unaffected by the evolve-and-measure cycles. If these eigenvalues are sufficiently close to unity, we may have $\Phi^n \rho_S \approx \rho_S$ for large values of n to a good approximation. We refer to the such states as *almost-fixed points* of Φ . We will illustrate

³Note that this method generalizes straightforwardly to the case where Φ is defective since the channel will still admit a Jordan Normal Form [15].

⁴Based on our numerical studies, we expect this situation to arise only rarely. Nevertheless, it may arise—at least approximately—from special, finely-tuned parameters, much like the almost-fixed points discussed below.

with a simple model how the quantum Zeno effect can be understood in terms of these fixed and almost-fixed points.

3.3 A Qubit Model

To illustrate how the QZE can be understood in terms of fixed points and almost-fixed points, we consider a model where both the system and the detectors are qubits. For simplicity, we take S and D to have the same energy gap, i.e., we take their free Hamiltonians to be $H_S = H_D = \hbar\omega\sigma_z$. We suppose that the S - D interactions are described by a transversal coupling of the form $H_{SD} = \hbar g \sigma_x \otimes \sigma_x$, and that the detectors are all prepared in their (free) ground state: $\rho_D = |0\rangle\langle 0|$. (We will later discuss the impact of different initial detector states.) While the main purpose of this model is to illustrate more general concepts, we note that it also describes certain physical settings which can arise, for instance, in circuit quantum electrodynamics (QED) [29, 73] or when dipole-dipole couplings are present [33]. The channel Φ will now depend on four parameters (namely g , ω , δt_F , and δt_M), which is why we do not explicitly write its functional dependence.

3.3.1 Recovering the conventional QZE as a special case

We begin by examining this model in an idealized limit to show that it encompasses the conventional quantum Zeno effect, though we will later relax our idealizations. In particular, we consider here the usual limit of infinite measurement frequency, which corresponds to $\delta t_F, \delta t_M \rightarrow 0$. In order to keep the measurements strong, i.e., to keep their impact appreciable as their duration becomes vanishingly short, we allow the S - D coupling strength to grow as the measurement duration decreases by keeping $g\delta t_M$ fixed in the limit. We will see in Chapters 4 and 5 that resulting system dynamics is very different if the coupling strength remains finite in the same limit.

To characterize the effect of many evolve-and-measure cycles on the system in the limit of rapid strong measurements, we find the eigenpairs of the channel Φ in this limit, shown in Table 3.2. We observe that in the limit, the eigenvectors are the identity matrix and the Pauli operators. That is, if the system is initially prepared in the state $\rho_S(0) = \frac{1}{2}(I + \vec{r} \cdot \vec{\sigma})$, after n cycles its state will be

$$\rho_S(n\delta t) = \frac{1}{2} \left(\lambda_0^n I + \sum_{j=1}^3 \lambda_j^n r_j \sigma_j \right), \quad (3.12)$$

where the eigenvalues of Φ are given in Table 3.2. Recall that δt_F and δt_M are taken to be vanishingly small here, so $\lambda_1 \rightarrow 1$ in the limit, while λ_2 and λ_3 do not generically approach unity (nor any value of special significance).

Eigenvalues	Eigenvectors
$\lambda_0 = 1$ for all parameter values	$V_0 \rightarrow I$
$\lambda_1 = 1 + \text{quadratic terms}$	$V_1 \rightarrow \sigma_x$
$\lambda_2 = \cos(2g \delta t_M) + \text{quadratic terms}$	$V_2 \rightarrow \sigma_y$
$\lambda_3 = \cos(2g \delta t_M) + \text{quadratic terms}$	$V_3 \rightarrow \sigma_z$

Table 3.2: Eigenvalues and eigenvectors of the channel Φ , which describes the effect of one cycle on the qubit system in our RIS model. The eigenpairs are given in the limit of $\delta t_F, \delta t_M \rightarrow 0$, with $g \delta t_M = \text{const.}$ The ‘quadratic terms’ in the left hand columns are terms which vanish in this limit as $\mathcal{O}(\delta t_F^2)$, $\mathcal{O}(\delta t_M^2)$, or $\mathcal{O}(\delta t_F \delta t_M)$, with no dependence on g .

Let us note the main features of this result:

1. The maximally mixed state of S is a fixed point of Φ , as one might expect from decoherence-like effects that could arise due to interactions with a succession of detectors which form a sort of structured environment for the system.
2. The σ_y and σ_z components of the initial system state $\rho_S(0)$ are exponentially suppressed by rapidly repeated strong measurements since $|\lambda_2|, |\lambda_3| < 1$ generically.
3. We have $\lambda_1 \rightarrow 1$ quadratically as $\delta t_F, \delta t_M \rightarrow 0$. This behaviour implies that the σ_x component of $\rho_S(0)$ is preserved in the limit of strong measurements performed at a high frequency. That is, states on the x -axis of the system’s Bloch sphere become frozen by the measurements in the high frequency limit, even though these states would exhibit non-trivial dynamics if left to evolve freely under H_S . This is the same phenomenon observed in Example 3.1—our model therefore encompasses as a special case the conventional quantum Zeno effect.
4. The fact that this model—which treats measurement as a purely dynamical process—exactly reproduces the freezing of $\rho_S = \frac{1}{2}(I + \epsilon \sigma_x)$ states which arose in Example 3.1 through projective σ_x measurements hints that the S - D measurements here somehow also measure σ_x on the system. Indeed, choosing $g \delta t_M = \pi(2k + 1)/4$ for integer k , the effect of Φ on a general system state is

$$\begin{pmatrix} a & b \\ b^* & c \end{pmatrix}_{[X]} \mapsto \begin{pmatrix} a & 0 \\ 0 & c \end{pmatrix}_{[X]} \quad (3.13)$$

in the $X := \{|\pm\rangle\}$ (i.e., Hadamard) basis. This is exactly the process described in Eq. (3.5): a projective σ_x measurement. Moreover, one can show that for these values of $g\delta t_M$, the σ_x component of the system’s Bloch vector becomes encoded in the detector’s post-measurement state. Moving away from the fine-tuned values of $g\delta t_M$ which produce (3.13) leads to weaker (i.e., non-projective) σ_x measurements of S , which encode $\langle\sigma_x\rangle$ of the system into the detector, multiplied by an attenuating factor describing the reduced transfer of information in weaker measurements.

5. Notice that λ_1 approaches unity—i.e., the QZE still occurs—even when $g\delta t_M$ has not been fine-tuned to produce projective measurements on the system. Thus, we see explicitly that the idealization of perfect projective measurements is not necessary to produce a perfect Zeno effect (in the sense that states can be perfectly preserved with weaker measurements). In fact, one can find numerous values of $g\delta t_M$ which cause the quadratic terms in λ_1 to vanish, thus making this eigenvalue approach unity even faster in the $\delta t_F, \delta t_M \rightarrow 0$ limit. This enhanced convergence yields a stronger Zeno effect, in that one gets nearer-to-perfect state freezing with lower measurement frequency (i.e., more favourable scaling). Intriguingly, these values of $g\delta t_M$ which accelerate the $\lambda_1 \rightarrow 1$ convergence are not generically the same ones that yield the projective measurement described in (3.13). In other words, “imperfect” (i.e., non-projective) measurements can produce a stronger Zeno effect, as we will see in detail in the following section.

3.3.2 Realistic settings

In experiments, the frequency with which one can repeat measurements is obviously limited, as is the coupling strength between systems and detectors. We will therefore now relax the typical idealizations of the quantum Zeno effect, made also in Section 3.3.1 by taking the $\delta t_F, \delta t_M \rightarrow 0$ limit, and move into more experimentally-relevant regimes. As in the previous section, we will proceed by analysing the eigenpairs of the channel Φ , now for a finite measurement frequency and a finite coupling strength.

Unsurprisingly, the eigenvalues and eigenvectors of Φ for realistic parameters are far more involved than those in the idealized limit we considered previously. In particular, the

eigenvectors have the form

$$\begin{aligned}
 V_0 &= \begin{pmatrix} a & 0 \\ 0 & 1-a \end{pmatrix}_{[Z]} & V_1 &= \begin{pmatrix} 0 & \theta \\ \varphi & 0 \end{pmatrix}_{[Z]} \\
 V_2 &= \begin{pmatrix} 0 & \xi \\ \eta & 0 \end{pmatrix}_{[Z]} & V_3 &= \begin{pmatrix} b & 0 \\ 0 & -c \end{pmatrix}_{[Z]}
 \end{aligned} \tag{3.14}$$

in the $Z = \{|0\rangle, |1\rangle\}$ basis, where a, b and c are non-negative and all Greek letters represent complex values. The full form of these matrices is discussed in Appendix A. Note that as $\delta t_F, \delta t_M \rightarrow 0$ for $g \delta t_M = \text{const}$, the above matrices tend towards those listed in Table 3.2, by definition of the latter. Two of the corresponding eigenvalues are

$$\lambda_0 = 1 \qquad \lambda_3 = \cos^2(g \delta t_M) - \frac{g}{\Omega} \sin^2(\Omega \delta t_M), \tag{3.15}$$

where $\Omega := \sqrt{g^2 + 4\omega^2}$. The expressions for the λ_1 and λ_2 are lengthy and are discussed in Appendix A, although the behaviour of these eigenvalues is described below. Note that in the limit $\delta t_F, \delta t_M \rightarrow 0$ for $g \delta t_M = \text{const}$, the eigenvalues also tend towards the values listed in Table 3.2, again, by definition. Observe that, as usual, any system density matrix can generically be decomposed into a weighted sum of V_0, \dots, V_3 . However, V_j does not represent a valid density matrix when considered alone, with the exception of V_0 .

For finite values of the model parameters, all eigenvalues and eigenvectors of Φ , except for λ_0 , depend non-trivially on $g, \omega, \delta t_F$, and δt_M . We present here their emergent features analogously to how we analysed the high frequency limit in Section 3.3.1:

1. The eigenvalue $\lambda_0 = 1$ is unique in that it is independent of all model parameters. It guarantees that Φ always has at least one fixed point, V_0 , as required by Brouwer's theorem. Correspondingly, we will refer to V_0 as the ‘‘Brouwer fixed point’’. Note that V_0 is always a valid density matrix, and perhaps surprisingly, it need not be the maximally mixed state (although we saw that it tends towards the maximally mixed state in the high measurement frequency limit). That is, for finite parameter values, the Brouwer fixed point state V_0 can lie anywhere on the z -axis of the system's Bloch sphere depending on $g, \omega, \delta t_F$, and δt_M .
2. Generically $|\lambda_3| < 1$, although as per Eq. (3.15), it is possible to have $\lambda_3 = 1$ for isolated parameter values. If $|\lambda_3| < 1$, the σ_z component of the system will be exponentially suppressed towards V_0 , whereas when $\lambda_3 = 1$ the σ_z component is preserved by the repeated cycles.

3. The matrices V_1 and V_2 describe the off-diagonal elements of the system's density matrix in the Z basis. As we saw in the previous section, they tend to σ_x and σ_y respectively in the limit of infinitely frequent strong measurements. In this limit $\lambda_1 \rightarrow 1$ quadratically, so the σ_x component of $\rho_S(0)$ is preserved in what amounts to an instance of the conventional QZE. We also found in Section 3.3.1 that for large *but finite* measurement frequencies, $|\lambda_1| < 1$ generically; that is, system states on the x -axis of the Bloch sphere are at best almost-fixed points of Φ when $\delta t_F, \delta t_M$ are infinitesimal but non-zero. This tells us that initial system states of the form $\rho_S(0) = \frac{1}{2}(I + \epsilon\sigma_x)$ are only approximately preserved by measurements repeated at generic high but finite frequencies, in agreement with experimental realizations of the QZE [51, 34]. In contrast with the usual Zeno calculation, our model easily allows us to determine to which state the system is ultimately driven upon escaping its QZE confinement: generically, it tends towards the Brouwer fixed point V_0 due to the repeated measurements.

Crucially, while $|\lambda_1|, |\lambda_2| < 1$ for generic values of $g, \omega, \delta t_F$ and δt_M (since Φ is CPTP), a numerical study of these eigenvalues reveals that there exist families of parameters for which λ_1 and λ_2 (separately) come arbitrarily close to, or reach unity. These parameters, shown in Fig. 3.1a, correspond to *finite measurement frequencies and a finite coupling strength*. For such special parameter values, linear combinations of V_0 and V_1 or V_0 and V_2 will be either fixed points or almost-fixed points of Φ . (We cannot distinguish between $\lambda_{1,2} \approx 1$ and $\lambda_{1,2} = 1$ numerically, so we will be conservative and assume only approximate equality, i.e., that these special parameters produce almost-fixed points.) That is, if the system is initially prepared in one of these linear combinations, its state will be near-perfectly preserved by the repeated measurements, despite the fact that these are not performed in the typical Zeno limit. We refer to these families of almost-fixed points as Zeno-like fixed points.

Linear combinations of V_0 and V_1 or V_0 and V_2 correspond to lines through the Bloch sphere which run parallel to the xy -plane (i.e., they are normal to the z -axis). One-dimensional families of Zeno-like fixed points produced by special combinations of parameters are shown in Fig. 3.1b for different values of $(g, \omega, \delta t_F, \delta t_M)$. Notice that these states cover the entire xy -plane: this coverage indicates that repeated measurements with a single type of detector (specifically, with detectors prepared in the same initial state $\rho_D = |0\rangle\langle 0|$) can preserve any state on the equatorial disk of the system's Bloch sphere, provided the measurement parameters are tuned properly. This is in marked contrast with the usual quantum Zeno effect, where only a single family of states can be frozen by a given kind of measurement.

Finally, the ability to choose a different initial state for the detectors provides even

greater flexibility in choosing which system states to freeze. Using a different ρ_D than $|0\rangle\langle 0|$ would move the Zeno-like fixed points in Fig. 3.1b out of the xy -plane. What is more, choosing a different ρ_D can move the Brouwer-guaranteed fixed point V_0 off of the z -axis to *any point on the system's Bloch sphere*, as shown in Fig. 3.1c, even when the parameters are not fine-tuned to yield Zeno-like fixed points. While the Brouwer fixed point does not directly underpin the QZE (as we discuss below), the ability to place V_0 anywhere in the Bloch sphere, and therefore to freeze any state of S , is a dramatic improvement over the traditional quantum Zeno effect. Finally, note that for generic parameter values, any initial system state will eventually be drawn towards this Brouwer fixed point.

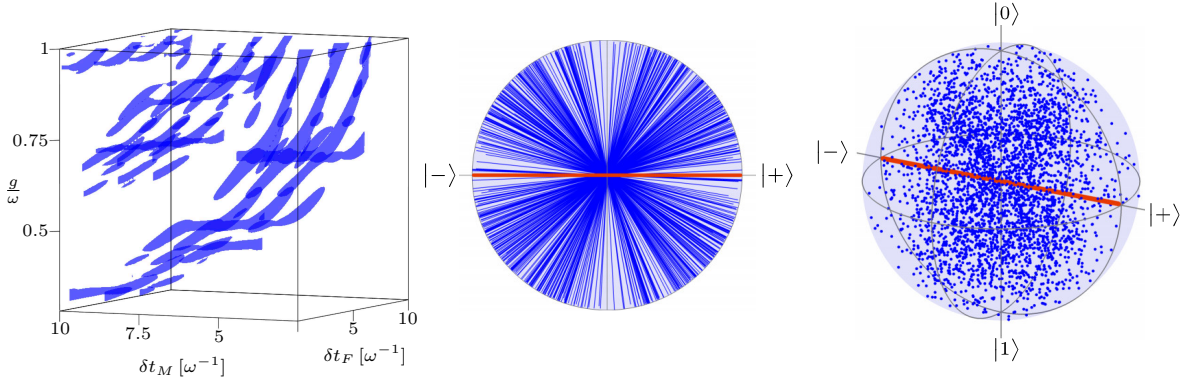


Figure 3.1: **a)** Location of the Zeno-like fixed points in the 3-dimensional parameter space. Plotted are the neighbourhoods in which the eigenvalue λ_2 differs from 1 by at most 10^{-2} . The thickness of these neighbourhoods illustrates the level of fine-tuning required to realize Zeno-like fixed points with this accuracy. **b)** Top view of the Bloch sphere. Locations of Zeno-like fixed point states (where $\lambda_1 = 1$ or $\lambda_2 = 1$) are in blue. They are highly concentrated on the xy plane. States preserved by the conventional Zeno effect are shown as a horizontal bold red line. **c)** Bloch sphere locations of target states preserved by Brouwer fixed points ($\lambda_0 = 1$) when the initial state of the detectors is arbitrarily varied, while being held fixed for each set of repeated measurements. We see that by varying the choice for the initial state of the detectors, the fixed points cover the full sphere isotropically about the z -axis. For comparison, the bold red line on the x -axis shows the states that can be preserved by the conventional QZE.

3.4 The S - D Interaction as a Measurement

Recall that we have raised the Heisenberg cut and described our detectors quantum mechanically. In doing so, we have modelled each measurement not just as a purely dynamical process, but as a unitary process. That is, we have not invoked any form of wavefunction collapse, be it through a measurement postulate or through the decohering action of an environment, as it is not needed to produce any of the effects discussed in Section 3.3. For the purpose of examining Zeno phenomenology, there is no reason to think of our measurements as collapsing the system to any post-measurement state, or a probabilistic mixture of such states, as is done with projective measurements. Nevertheless, one could imagine the used detectors in our model going on to interact with an environment which induces in them a quantum-to-classical transition. Such a scenario would make a “collapse” interpretation reasonable. For illustration then, we briefly sketch how our measurements can be understood in the usual language of measurement operators and positive-operator valued measures (POVMs).

To cast our dynamical measurements in terms of POVMs, we will require that the latter description produce the same system state-update rule as Φ . The channel Φ admits an operator-sum representation of the form

$$\Phi(\rho_S) = \sum_j K_j \rho_S K_j^\dagger, \quad (3.16)$$

where $\{K_j\}$ are known as *Kraus operators*. Defining $E_j = K_j^\dagger K_j$, it follows immediately that $\sum_j E_j = I$, $E_j = E_j^\dagger$, and $E_j \geq 0$. Thus, $\{E_j\}$ constitutes a POVM (see [80] for an introduction to Kraus operators and POVMs), where the probability of the j -th outcome is given by

$$p_j = \text{tr}(E_j \rho_S), \quad (3.17)$$

and the post-measurement system state corresponding to this outcome is

$$\rho_S^{(j)} = \frac{K_j \rho_S K_j^\dagger}{p_j}. \quad (3.18)$$

We see, then, that the action of the channel Φ can be understood as

$$\Phi \rho_S = \sum_j p_j \rho_S^{(j)}, \quad (3.19)$$

that is, as mapping an initial system state to a probabilistic mixture of post-measurement states, as in Eqs. (3.5) and (3.13). Note finally that the choice of Kraus operators, and

therefore of POVMs, is not unique: there exist a family of operators $\{K_j\}$ which will produce the same state-update rule but will yield a corresponding family of distinct POVMs. The question of which Kraus operators / POVM to use must be decided by factors external to the present model: for instance, the particular decohering action of an environment on D and/or S . Nevertheless, for illustration we give possible POVMs for Φ corresponding to the two parameter regimes discussed above.

3.4.1 An idealized example

In the case of the conventional Zeno limit presented in Section 3.3.1 with $g\delta t_M$ tuned to yield projective measurements, the channel Φ defined by Eq. (3.13) can be decomposed into the Kraus operators

$$K_+ = |+\rangle\langle+| \quad K_- = |-\rangle\langle-|. \quad (3.20)$$

We can therefore interpret Φ as a dephasing channel [48]. Because K_+ and K_- are orthogonal projectors, we have that $\{E_\pm\} = \{K_\pm\}$, as one would expect since this channel is known to describe a projective σ_x measurement.

3.4.2 A realistic example

We now consider a more realistic example, where a finite measurement duration and coupling strength produce a Zeno-like fixed point. In particular, for parameters

$$\delta t_F = 15.13\omega^{-1} \quad \delta t_M = 14.96\omega^{-1} \quad \frac{g}{\omega} = 0.865 \quad (3.21)$$

the channel Φ has eigenvectors

$$\begin{aligned} V_0 &= \begin{pmatrix} 0.5 & 0 \\ 0 & 0.5 \end{pmatrix} & V_1 &= \begin{pmatrix} 1.0 & 0 \\ 0 & -1.0 \end{pmatrix} \\ V_2 &= \begin{pmatrix} 0 & 0.42 - 0.27i \\ 0.42 + 0.27i & 0 \end{pmatrix} & V_3 &= \begin{pmatrix} 0 & 0.27 + 0.42i \\ 0.24 - 0.42i & 0 \end{pmatrix}, \end{aligned} \quad (3.22)$$

and eigenvalues

$$\lambda_0 = 1.0 \quad \lambda_1 = 0.73 \quad \lambda_2 = 1.0 \quad \lambda_3 = 0.73. \quad (3.23)$$

Thus, the one-dimensional family of Zeno-like fixed points $\rho_S(0) = \frac{1}{2}(V_0 + \epsilon V_2)$ is perfectly preserved (to numerical precision) by the repeated measurements due to the Zeno-like effect arising from the parameters in Eq. (3.21).

A Kraus decomposition of the channel Φ for these parameters is given by

$$K_{\pm} = (0.36 + 0.55i)I \pm (0.22\sigma_x + 0.14\sigma_y). \quad (3.24)$$

One can readily check that the values in Eqs. (3.22)–(3.24) are stable under small perturbations of the parameters in Eq. (3.21). Notice that Φ does not correspond to a projective measurement in this case; instead, it is described by the POVM elements

$$E_{\pm} = \frac{1}{2}(I \pm \vec{n} \cdot \vec{\sigma}) \quad (3.25)$$

where $\vec{n} = (0.32, 0.20, 0)$.

3.5 Discussion

We conclude based on the results in this chapter that the quantum Zeno effect—at least for qubits—is a special case of a more general Zeno phenomenon in which a system can be effectively frozen by repeated measurements which need not be perfect, and which need not be repeated at an infinite frequency. Moreover, this more general phenomenon allows greater flexibility than the conventional QZE in terms of which states can be frozen by the measurements. In our particular model, any state on the system’s Bloch sphere could be frozen with a fixed type of system-detector coupling, in contrast with the conventional QZE.

Generically, imperfect measurements repeated at a finite frequency, of course, do not freeze a quantum system. However, we found that for special combinations of parameters describing the measurements, we could preserve families of system states to an arbitrary degree, provided the parameters could be sufficiently fine-tuned. The conventional QZE is simply a particular case of this Zeno-like phenomenon, produced by parameters that correspond to an infinite measurement frequency (in our model this meant $\delta t_F, \delta t_M \rightarrow 0$, $g \delta t_M = \text{const}$). The prospect of experimentally achieving a strong Zeno-like effect through realistic parameter values—as opposed to the fundamentally inaccessible limit of infinite measurement frequency that has so far been pursued—is intriguing.

When the measurement parameters are not specially chosen to produce Zeno-like fixed points, the system is driven towards an attractive fixed point (V_0 in our notation) exponentially in n , the number of measurements. We showed the general existence of this attractive

fixed point using Brouwer’s theorem, and showed that it need not be maximally mixed. Rather, in our simple model, it could be placed anywhere on the Bloch sphere by initializing the detectors in a suitable state ρ_D . This attractive fixed point, whose existence does not depend on fine-tuning of the measurement parameters, could also be used for state preservation (e.g., in a quantum memory), or even for state preparation. In experiments, whether Zeno-like or Brouwer fixed points are more readily implementable depends on how precisely the measurement parameters can be set and the initial detector state prepared, and on what parameter range is experimentally accessible.

The Zeno-like fixed points can be understood in the same way as the conventional Zeno effect, since the latter is a special case of the former. The intuition behind the Brouwer fixed points, however, is different: Imagine a piece of metal being repeatedly struck by a succession of cold hammers. On one hand, the violent nature of the striking should warm up the metal, but on the other, the low temperature of the hammers should cool it down. Neglecting transients, as we have done in this chapter (see Sections 4.4.2 and 5.4 for an analysis of transient effects), one expects the metal piece in this analogy to approach a fixed point equilibrium. Likewise, the system in our model is rapidly coupled to a succession of cold detectors. The rapid coupling and decoupling might be expected to disturb the system, while the contact with cold detectors might be expected to cool it. Together, these two factors drive the system towards a fixed point that is generally not a thermal equilibrium state. It is this fixed point that is guaranteed by Brouwer’s theorem.

While we have used a simple model for illustration, we expect the general phenomena observed here [which arose due to the nature of $\text{spec}(\Phi)$] to be present also in more complex systems. Consider, for example, the setup of entanglement farming from an optical cavity field [75]. There, identically prepared unentangled pairs of atoms are successively sent through an optical cavity. The successive pairs of atoms were observed to drive the cavity field towards a certain entangling state. While no connection to the Zeno effect was made in Ref. [75], we can now see that this entangling state is likely an instance of a Zeno-like fixed point, with each pair of atoms playing the role of a detector and the cavity field being the system. Moreover, the universal existence of a fixed point is very general: it is guaranteed for higher-dimensional systems by Brouwer’s theorem [16], and even for infinite dimensional systems from Schauder’s theorem [88].

Finally, let us remark that the interactions in a RIS model such as the one considered here can not only slow down, but also speed up the dynamics of a system. This can be understood as a manifestation of the *anti-Zeno effect*, wherein repeated measurements accelerate system dynamics [60, 34]. This effect is most clearly seen using the formalism of the following chapter.

Chapter 4

Indirect Quantum Control: Coherent Control

In this chapter we present the material published in [65], building upon the formalism introduced in Chapter 3.

4.1 Motivation

As was discussed in Chapters 1 and 2, the ability to control quantum systems in a precise and predetermined way is an essential component of most proposed quantum technologies. Typically, one seeks to control systems coherently, i.e., unitarily. However, the manifestly open nature of most real quantum systems, and the dissipation it introduces, complicates this goal. While there exist high-level methods of dealing with dissipation-induced errors, such as quantum error correction which operates on the level of quantum “software”, it remains advantageous to control a quantum system rapidly as compared to the dissipation timescales. Such a hardware-level achievement can greatly improve the performance of these higher-level techniques (for instance, by reducing the average number of errors per physical gate in quantum error correction). However, improving the ratio between control timescales and coherence times is often difficult, as both timescales depend on the strength of the system-environment coupling.

The typical approach to quantum control involves driving a quantum system directly, and in doing so, modifying its Hamiltonian in a time-dependent manner, as in Eq. (2.8). In many implementations, this driving is achieved by applying carefully shaped and timed

electromagnetic (EM) pulses to the system. The system's response is usually modelled semi-classically, yielding a dynamics generated by (2.8). We refer to this approach as *direct control*. The stronger the coupling between the system and this EM control field, the larger the resulting control Hamiltonian $H_c(t)$ in magnitude, and the faster a control operation can be performed. However, this EM field, by definition, constitutes part of the system's environment. This is illustrated schematically in Fig. 4.1a. Therefore, strong coupling to this field generically means strong coupling to the environment, which is associated with shorter coherence times. Since both the control timescales and the coherence times of the system depend on the system-environment coupling, it can be difficult to improve the ratio of these timescales. There are various methods for improving this ratio while still employing direct control, including fabrication techniques which effectively create a less noisy environment [104], or engineered system-environment couplings which allow control pulses to reach the system but attenuate environmental noise [53].

Example 4.1: Direct Control. Suppose S is a quantum harmonic oscillator which is classically driven by a control field, resulting in a Hamiltonian

$$H(t) = \underbrace{\hbar\nu a^\dagger a}_{H_S} + \underbrace{V(t)(a + a^\dagger)}_{H_c(t)}. \quad (4.1)$$

A typical problem of direct quantum control is to determine $V(t)$ so as to produce some unitary U on the system.

In this chapter we will examine a different approach, known as *indirect control*. The idea of indirect control is to introduce an auxiliary system which we call the *actuator* (a term borrowed from classical control theory), denoted A , which is coupled to the system S . Then, one performs operations on S not by addressing it directly, but rather, by driving A and exploiting the S - A coupling to indirectly affect the system. Such a strategy is particularly appealing in settings where the actuator can be controlled rapidly (via a strong coupling to the environment), and where the system has long coherence times (due to a weak coupling to the environment). This setting, which can occur naturally [1] or can be engineered [89], is illustrated schematically in Fig. 4.1b.

Example 4.2: Indirect Control. Suppose that S is a quantum harmonic oscillator, that A is a qubit, and that the pair's Hamiltonian has the form

$$H(t) = \underbrace{\hbar\nu a^\dagger a}_{H_S} + \underbrace{\frac{\hbar\omega}{2}\sigma_z}_{H_A} + \underbrace{\hbar g X \otimes (\vec{n} \cdot \vec{\sigma})}_{H_{SA}} + \underbrace{\vec{V}(t) \cdot \vec{\sigma}}_{H_c(t)}, \quad (4.2)$$

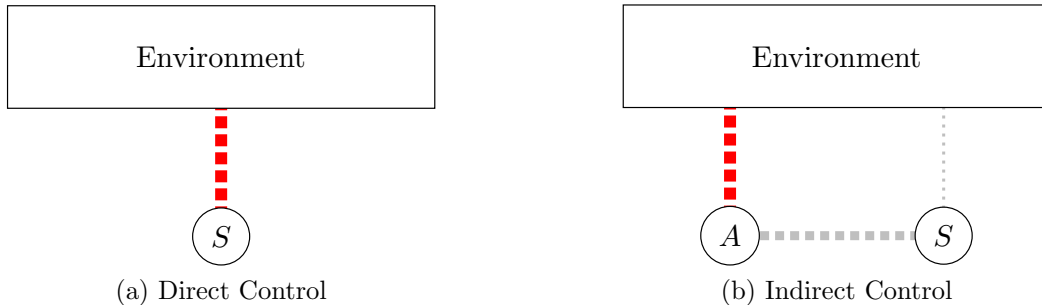


Figure 4.1: Schematic illustrations of direct control and indirect control. In both cases, the environment is taken to include the classical controller (e.g., the EM control field) used to steer either S or A . The thickness of the dashed lines is meant to denote coupling strength, with a thick line indicating a strong coupling. The red colour is used to indicate which coupling is used to drive either S or A .

where $X = (a + a^\dagger)/2$ is a quadrature operator on S and $\vec{\sigma} = (\sigma_x, \sigma_y, \sigma_z)$. For different choices of \vec{n} , Eq. (4.2) describes several objects amenable to indirect quantum control: for example, a nanomechanical resonator coupled to a superconducting qubit [50, 52, 63] or to an electron spin [83], as well as circuit (cavity) quantum electrodynamics setups, where an electromagnetic field mode couples to superconducting qubits (atoms). A typical problem of indirect quantum control is to determine the pulse $\vec{V}(t)$ on A so as to produce some unitary U on S .

Indirect control appears to offer the “best of both worlds” in terms of environmental coupling: rapid control of the system, limited by the actuator-environment coupling strength (which could be made strong), and long system coherence times, determined by the system-environment coupling strength (which could be made weak). Moreover, it has been shown that full control of A typically yields universal control of S [72, 71]. However, indirect control involves some appreciable difficulties as compared to direct control. In particular:

1. It can be very difficult to find the right pulses. To see why, think of casting indirect control as a direct control problem, where the entire S - A object is to be steered via an EM control field that couples only (or at least primarily) to A . Generically, the Hilbert space of S - A is significantly larger than that of S , and so finding appropriate pulses (say, using GRAPE) on A to produce a desired effect on S can be significantly

more difficult than finding pulses to apply directly to S .

2. Closely related to the first point, indirect control introduces the possibility for incoherent error on S beyond environmentally-induced dissipation. Concretely, an imperfectly calibrated pulse applied directly to S will produce a coherent error, i.e., its effect will be unitary (modulo decoherence), but it will not quite be the intended unitary. On the other hand, the same error when driving A can not only implement the wrong unitary on S , but it will generically leave S and A entangled, producing a net non-unitary effect on S . Indirect control can therefore “artificially” increase the potential for incoherent errors.

Despite these difficulties, indirect control schemes have shown promise in a variety of settings, including spin chains [22, 23, 45], superconducting qubits [95], nanomechanical resonators [52, 83], and perhaps most notably, in nuclear/electron spin systems [76, 77, 47, 24, 97, 1]. However, given the difficulty in finding control pulses on A which will produce a desired unitary on S , implementations (or proposed implementations) of indirect control to date have exploited special structures of particular S - A Hamiltonians on a case-by-case basis depending on the type of system and actuator at hand.

4.1.1 An existing indirect control scheme

One particular indirect control scheme is popular in physical settings where a nuclear spin (S) couples to an electron spin (A), such as nitrogen-vacancy (NV) centres and electron spin resonance (ESR) systems. These have Hamiltonians that can often be cast in the form

$$H = \sum_j H_S^{(j)} \otimes |j\rangle\langle j|_A, \quad (4.3)$$

where $\{|j\rangle\}$ are orthogonal actuator states. By preparing A in a state $|j\rangle$, one can implement unitary evolution by $H_S^{(j)}$ on the system. Then, by rapidly flipping the actuator between these special states $\{|j\rangle\}$, one can indirectly implement different unitary dynamics on the system. This approach effectively reduces the indirect control problem for these particular settings to one of direct control: One simply has to find a sequence of Hamiltonians on S (choosing from the set $\{H_S^{(j)}\}$) to produce a desired unitary [69]. The difference between this scheme and direct control is simply that the different Hamiltonians on S are implemented by varying the state of A , rather than by driving S directly. Note that because A is flipped only between a discrete set of states in this scheme, we have not explicitly shown the $H_c(t)$ term describing the driving of A in Eq. (4.3).

Notice that the approach described above relies crucially on the special structure of (4.3) to produce unitary dynamics on S conditioned on the state of A . Generic Hamiltonians, however, do not have this special structure, meaning that this particular indirect control scheme is not generally applicable. We now present an indirect control scheme which, to our knowledge, is the first one to reduce the general problem of indirect control to that of direct control (analogously to the scheme above) *for any system and actuator, regardless of their overall Hamiltonian*. We will introduce this scheme using formalism developed in the previous chapter.

4.2 The Scheme

Our scheme is built upon an emergent feature of RIS dynamics. We will first introduce this feature in general terms and then show how it can be used to produce a universal scheme for indirect control.

Consider a quantum system S and a quantum actuator A , initially in a product state $\rho(0) = \rho_S(0) \otimes \rho_A$. Suppose that the actuator is periodically reset to the state ρ_A with a period δt . For convenience, we will assume the resets to be instantaneous and the cycles to be of uniform duration, although we will see later that neither of these assumptions are truly necessary. Note that this constitutes an RIS model as in Chapter 3, although here we interpret the ancilla as an actuator rather than as a detector. Moreover, it is more useful here to think of a single actuator being periodically reset, rather than identically-prepared ancillas being drawn from a reservoir.

Between successive actuator resets, S - A is taken to evolve according to the Lindblad equation

$$\frac{d\rho(\tau)}{d\tau} = \mathcal{L}(\tau)\rho(\tau), \quad (4.4)$$

where we decompose the Liouvillian into parts acting non-trivially only on S , A , and S - A :

$$\mathcal{L}(\tau) = \mathcal{L}_S + \mathcal{L}_A + \mathcal{L}_{SA}(\tau/\delta t), \quad (4.5)$$

To illustrate the effect of time dependence in \mathcal{L} we allow \mathcal{L}_{SA} to vary in time (notice that we have normalized its argument by δt for mathematical convenience). However, considering more general time dependence requires only trivial modifications to the steps described below.

To facilitate comparison with existing control schemes, we will be particularly interested in the special case where S - A is closed and evolves unitarily between resets. Moreover, we

will suppose that the time dependence in the interaction Hamiltonian is fully described by a piecewise-continuous switching function g . In this case, we have

$$\mathcal{L}(\tau) = -\frac{i}{\hbar}[H_S + H_A + g(\tau/\delta t)H_{SA}, \cdot]. \quad (4.6)$$

We now define a dynamical map $\Phi(\delta t)$ on S , which describes the effect of evolution by $\mathcal{L}(t)$ between subsequent resets. Concretely, we have that $\Phi(\delta t)$ acts on a system density operator as

$$\Phi(\delta t) \cdot = \text{tr}_A \left\{ \mathcal{T} \exp \left[\int_0^{\delta t} d\tau \mathcal{L}(\tau) \right] (\cdot \otimes \rho_A) \right\}. \quad (4.7)$$

We may then write the system's state after one cycle as $\rho_S(\delta t) = \Phi(\delta t)\rho(0)$, and its state after n cycles have been performed in a time t (for integer n) as $\rho_S(t) = \Phi(t/n)^n \rho_S(0)$, as in Chapter 3. The map $\Phi(\delta t)$ here is similar to the channel considered in Section 3.3, except for two main differences: (i) we now allow S - A to be an open bipartite object (i.e., with potentially dissipative dynamics between resets), and (ii) we have not made any assumptions here about the nature of S , A , or their aggregate Liouvillian. Note that, in contrast with the previous chapter, it will be convenient here to write explicitly the dependence of Φ on δt .

Our scheme will utilize cycles that are short as compared to the natural dynamics of S - A . We will therefore seek to expand $\rho_S(t)$ in powers of $1/n$, a small number when the actuator is reset at a high rate (for some nonzero t). In terms of the channel $\Phi(t/n)^n$, which describes the system's evolution over a time t when n actuator resets have been performed, we wish to find a series of the form

$$\Phi(t/n)^n = \Omega_0(t) + \frac{1}{n} \Omega_1(t) + \frac{1}{n^2} \Omega_2(t) + \dots \quad (4.8)$$

Here each $\Omega_j(t)$ is an unknown superoperator on the system with no dependence on n . Noting that $\mathcal{L}(\delta t \cdot \zeta) = \mathcal{L}_S + \mathcal{L}_A + \mathcal{L}_{SA}(\zeta)$ is independent of t [since the argument of \mathcal{L}_{SA} is scaled by δt , see Eq. (4.6)], we proceed by first expanding $\Phi(\delta t)$ asymptotically for small δt (compared to the natural dynamics of S - A) as

$$\Phi(\delta t) = I + \delta t \Phi_1 + \delta t^2 \Phi_2 + \dots, \quad (4.9)$$

where each Φ_k is a superoperator with no δt dependence. One can easily find the specific form of each Φ_k using a Dyson series. In particular:

$$\Phi_k \cdot = \text{tr}_A \int_0^1 d\zeta_1 \int_0^{\zeta_1} d\zeta_2 \dots \int_0^{\zeta_{k-1}} d\zeta_k \left[\prod_{j=1}^k \mathcal{L}(\delta t \cdot \zeta_j) \right] (\cdot \otimes \rho_A). \quad (4.10)$$

4.2.1 Mathematical intuition

Before analyzing Eq. (4.8) in detail and presenting our main result, let us first consider an analogous but simpler situation. In particular, consider a matrix $R(\theta) \in \text{SO}(2)$ representing a rotation by θ in \mathbb{R}^2 . The action of $R(\theta)$ can be obtained as the outcome of a series of infinitesimal rotations, each given by $I + \delta\theta R'(0) + \mathcal{O}(\delta\theta^2)$, for an arbitrary $\mathcal{O}(\delta\theta^2)$ term. Concretely, setting $\delta\theta = \theta/n$, we have

$$\left[I + \frac{\theta}{n} R'(0) + \mathcal{O}\left(\frac{\theta^2}{n^2}\right) \right]^n = \underbrace{e^{R'(0)\theta}}_{R(\theta)} + \mathcal{O}(1/n) \quad \text{for } n \gg 1. \quad (4.11)$$

The key observation here is that for large n (i.e., for sufficiently small $\delta\theta$) only the $\mathcal{O}(\delta\theta)$ term contributes to leading order, while the impact of any $\mathcal{O}(\delta\theta^2)$ term vanishes as $n \rightarrow \infty$ [37, 98].

Observe that $\Phi(t/n)^n$ can be expressed in a form very similar to the previous equation:

$$\Phi(t/n)^n = \left[I + \frac{t}{n} \Phi_1 + \mathcal{O}\left(\frac{t^2}{n^2}\right) \right]^n. \quad (4.12)$$

Based on the analogy involving rotations, one might expect that $\Phi(t/n)^n = e^{\Phi'(0)t} + \mathcal{O}(1/n)$, which, upon comparing with (4.8), would immediately yield an expression for $\Omega_0(t)$. [Notice from Eq. (4.9) that $\Phi'(0) = \Phi_1$.] We will see that this intuition is correct, and its physical consequences will underlie our indirect control scheme.

4.3 Main Result

The term $\Omega_0(t)$ is of special interest when the reset cycles are performed at a high rate, as it gives the leading-order description of the system's reduced dynamics. Mathematically, it describes $\Phi(t/n)^n$ in the limit of $n \rightarrow \infty$ for fixed t . As the mathematical intuition from rotations in \mathbb{R}^2 would suggest, we indeed have

$$\Omega_0(t) = \lim_{n \rightarrow \infty} \Phi(t/n)^n = e^{\Phi_1 t}. \quad (4.13)$$

Formally, this result is a direct consequence of Chernoff's theorem [26] (p. 241, see also [27, 28]), which requires that Φ be a continuous function of linear contractions on a Banach space, with $\Phi(0) = I$. We verify in Appendix B that Φ , as constructed, satisfies these

conditions under the induced trace norm on the set of self-adjoint trace-class operators acting on the system's Hilbert space.

We see from Eq. (4.10) for $k = 1$ that

$$\Phi_1 \cdot = \mathcal{L}_S + \text{tr}_A [\bar{\mathcal{L}}_{SA}(\cdot \otimes \rho_A)], \quad (4.14)$$

where $\bar{\mathcal{L}}_{SA} := \int_0^1 d\zeta \mathcal{L}_{SA}(\zeta)$ is the time average of \mathcal{L}_{SA} over one cycle. To better understand this result, let us first consider the case where S - A is closed, i.e., where the pair evolves unitarily between resets of A . In this case, Eq. (4.14) simplifies to

$$\Phi_1 \cdot = -\frac{i}{\hbar} \text{tr}_A [H_S + H_A + \bar{g} H_{SA}, \cdot \otimes \rho_A], \quad (4.15)$$

where $\bar{g} := \int_0^1 d\zeta g(\zeta)$. To simplify this equation, we use the fact that there exist operators $\{S_j\}$ and $\{A_j\}$ acting on the Hilbert spaces of the system and actuator respectively such that

$$H_S + H_A + \bar{g} H_{SA} = \sum_j S_j \otimes A_j. \quad (4.16)$$

We then have, for some operator X on the system's Hilbert space, that

$$\Phi_1 X = -\frac{i}{\hbar} \sum_j \text{tr}_A \left(S_j X \otimes A_j \rho_A - X S_j \otimes \rho_A A_j \right) \quad (4.17)$$

$$= -\frac{i}{\hbar} \sum_j \left(S_j X \text{tr}(A_j \rho_A) - X S_j \text{tr}(\rho_A A_j) \right)$$

$$= -\frac{i}{\hbar} \left[\sum_j S_j \text{tr}(A_j \rho_A), X \right]$$

$$= -\frac{i}{\hbar} \left[\text{tr}_A \left(\sum_j S_j \otimes A_j \rho_A \right), X \right]$$

$$= -\frac{i}{\hbar} [H_S + \bar{g} \text{tr}_A(H_{SA} \rho_A), X]. \quad (4.18)$$

This means that (4.15) can be written as

$$\Phi_1 \cdot = -\frac{i}{\hbar} [H_{\text{eff}}, \cdot], \quad (4.19)$$

where the *effective Hamiltonian* H_{eff} is given by

$$H_{\text{eff}} = H_S + \bar{g} \text{tr}_A(H_{SA} \rho_A). \quad (4.20)$$

Clearly $H_{\text{eff}}^\dagger = H_{\text{eff}}$, so to leading order in $1/n$, the system's reduced dynamics is unitary when S - A is closed, and is described by the von Neumann equation

$$\frac{d\rho_S}{dt} = -\frac{i}{\hbar}[H_{\text{eff}}, \rho_S] + \mathcal{O}(1/n). \quad (4.21)$$

This is a surprising result, since one component of a bipartite quantum object seldom evolves unitarily when both parts are coupled.

If, for instance, the system-actuator coupling is described by a separable interaction Hamiltonian $H_{SA} = B \otimes C$, the system's reduced dynamics will be well-described by $H_{\text{eff}} = H_S + \langle C \rangle B$, where $\langle C \rangle = \text{tr}(C\rho_A)$, when the reset rate is high. More generally, different types of coupling between S and A will lead to different effective Hamiltonians, generating unitary system dynamics conditioned upon ρ_A , in much the same way as in Section 4.1.1.

Let us now return to the general case where S - A is open. Just as a Hamiltonian H on S - A can be decomposed into system, actuator and interaction components, a Lindblad dissipator can also be decomposed as $\mathcal{D} = \mathcal{D}_S + \mathcal{D}_A + \mathcal{D}_{SA}$, where \mathcal{D}_S , \mathcal{D}_A and \mathcal{D}_{SA} act non-trivially only on S , A and S - A respectively. While the \mathcal{D}_{SA} term could in principle be quite general, most phenomenological models used to describe experiments have $\mathcal{D}_{SA} = 0$, effectively describing a dynamics in which the system and actuator dissipate separately into the environment (see, e.g., [36, 83, 95]). We will adopt this description of the system-actuator dynamics as well, and assume that the S - A dynamics between resets is generated by

$$\mathcal{L}(\tau) = -\frac{i}{\hbar}[H_S + H_A + g(\tau/\delta t)H_{SA}, \cdot] + \mathcal{D}_S + \mathcal{D}_A. \quad (4.22)$$

Under this assumption, the system's reduced dynamics is described, to leading order, by

$$\frac{d\rho_S}{dt} = \Phi_1\rho_S = [H_S + \text{tr}_A(H_{SA}\rho_A), \rho_S] + \mathcal{D}_S\rho_S(t) + \mathcal{O}(1/n). \quad (4.23)$$

Notice an interesting feature in Eq. (4.23): to leading order in $1/n$, the system's dissipator is unchanged by A ; that is, the actuator does not speed up the system's decoherence at this order. However, the Hamiltonian part of the system's dynamics *is* changed by A . It is on this feature that our indirect control scheme is based.

We see in Eq. (4.23) that the Hamiltonian part of the system's leading-order dynamics under frequent resets of A depends on ρ_A . That is, by choosing different states to which the actuator is repeatedly reset, one can implement entire families of H_{eff} . One can imagine resetting to a certain ρ_A for some period of time, and then to a different one, and so on, to

implement different effective Hamiltonians on S . Simply using this approach to implement a discrete set of effective Hamiltonians will generically yield universal coherent control of the system, provided the algebra generated by H_S and $\text{tr}(H_{SA}\rho_A)$ through commutation includes all possible Hamiltonians on the system, which is generically the case [69]. We will take this approach a step further, and imagine reinitializing A in a slightly different state with each cycle, instead of simply resetting it. This strategy is illustrated schematically in Fig. 4.2. Provided the variation in these initial actuator states is sufficiently slow as compared to the dynamics of S , the result will be to introduce time dependence into H_{eff} . Observe in Eq. (4.23) that this implies that, to order $\mathcal{O}(1)$, we can modify the system's effective Hamiltonian on a timescale that depends only on A (which could be rapidly controllable), whereas the system's dissipation depends only on its coupling to the environment (which could be weak). This technique of repeatedly initializing A in a predetermined sequence of states constitutes our indirect control scheme. Not only can it enable improvement in the ratio of control timescales to system coherence times, but it does so with (almost) no assumptions on the nature of S , A , or the coupling between them.

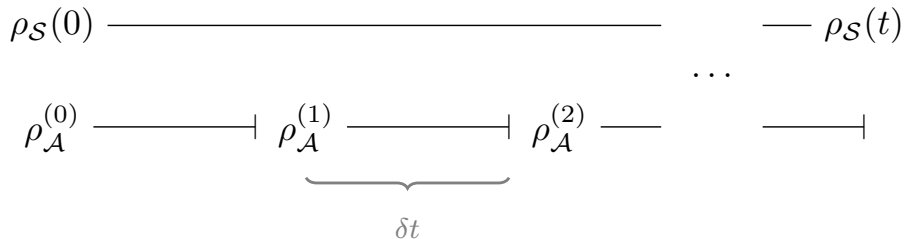


Figure 4.2: A schematic illustration of our scheme, where the actuator is reinitialized with a period δt to states $\rho_A^{(j)}$. The sequence $\{\rho_A^{(j)}\}_j$ should vary slowly from element to the next, such that $\rho_A^{(j)} \approx \rho_A^{(j+1)}$.

Notice that our scheme maps the potentially difficult (and often intractable) problem of indirect quantum control to that of direct control. Concretely, it allows one to indirectly implement a time-dependent effective Hamiltonian on S . Unlike with direct control, however, this Hamiltonian is not physically implemented by applying a suitable EM pulse directly to the system, but rather, by finding a suitable sequence of states $\{\rho_A^{(j)}\}$ in which to initialize the actuator. The problem of finding $\{\rho_A^{(j)}\}$ is equivalent to that of finding the right pulse to apply directly to S .

4.3.1 Relation to the quantum Zeno effect

We now take a moment to discuss the relation of our scheme, and more specifically the behaviour of $\Omega_0(t)$ when A is repeatedly reset to the same state ρ_A , to the quantum Zeno effect (QZE). While both share some common features, there are also important differences between them.

Both our scheme and the QZE involve frequent “kicks” to the system. In the case of the latter, these kicks are usually provided by measurements, although as we saw in Chapter 3, these measurements can be dynamical, and need not involve any sort of quantum-to-classical transition or collapse. Depending on one’s view of what exactly constitutes a Zeno effect, one could think of our scheme as being Zeno-like, in that it expands upon several features introduced in Section 3.3.2. One could interpret the eigenstates of H_{eff} , which are not generically eigenstates of the free system dynamics, as being preserved by a Zeno-like effect. One could also think of transitions which occur more quickly under H_{eff} than under H_S as being anti-Zeno-like.

There are, however, some inescapable difference between the phenomenon introduced in this chapter and the QZE. One such difference is philosophical: What is typically called the “Zeno effect” revolves around the *limit* of high measurement frequency. Our scheme, on the other hand, works in the *regime* of high reset frequencies, but explicitly avoids the limit. This important point will be further discussed below, and forms the basis of Chapter 5. Another reason is more physical: The limit considered in the conventional QZE is one in which an increasing number of measurements are performed within a fixed time interval. Crucially though, the nature of these measurements does not change—for instance, they do not weaken—as their frequency increases. Mathematically, this is reflected in the fact that the channel Φ describing one evolve-and-measure cycle of the QZE comes to describe a non-trivial measurement as $\delta t \rightarrow 0$. This can be modelled dynamically by letting the coupling strength grow unbounded, as in Section 3.3.1. Things are manifestly different in the present case, where we insist upon a finite coupling strength so as to model real experiments. In particular, the equality

$$\lim_{n \rightarrow \infty} \Phi(t/n)^n = e^{\Phi_1 t} \quad (4.24)$$

relies crucially on the fact that $\Phi \rightarrow I$ as $n \rightarrow \infty$ for fixed t (so $\delta t \rightarrow 0$). Physically, this means that the kicks given by A to S with each cycle become weaker as they become short. That is to say that the present phenomenon involves a different limit, or rather, a different regime, than the conventional quantum Zeno effect. This difference is clearly seen in Table 3.2, where the channel Φ manifestly does not tend towards I in the limit of rapid cycles.

Finally, let us mention recent results by Zanardi and Campos Venuti [108, 109] (see also [2]). These authors discovered a phenomenon closely related to the QZE, wherein unitary evolution, generated by a “dissipation-projected Hamiltonian,” can arise in an open system. While their results and ours may both stem from a common fundamental principle, Refs. [108, 109] rely upon a particular scaling that is not present in our scheme. Conversely, our results are concerned with the particular setup of a coupled system and actuator, whereas theirs are general statements about open quantum systems.

4.3.2 Interpretation

Why does the system’s Hamiltonian become modified to leading order by our scheme when its dissipator does not? One can view the actuator as giving a “kick” to S with each cycle. As we increase the number of cycles n within a time t , the kicks become weaker but also more numerous, as discussed above. These competing trends underpin our scheme: when the cycle duration δt is short, the effect of each cycle on S can be approximated as $\Phi(\delta t) \approx I + \delta t \Phi_1$. As per Section 4.2.1, for sufficiently short cycles the system’s leading-order reduced dynamics depends only on Φ_1 . Crucially though, Φ_1 generically describes a non-trivial but *non-entangling* operation on S - A . This is not unique to the present scheme: the non-entangling nature of Φ_1 is a generic feature of the first-order Dyson series term for a bipartite quantum object, and has been used in very different contexts (see, e.g., [74]). Our scheme, in other words, relies on the general phenomenon that two quantum objects interacting for a short time δt can impact each other faster than they can become significantly entangled. Therefore, by mimicking a series of short interactions between S and A through repeated resets (or more generally, reinitializations) of the latter, we can effectively modify the system’s Hamiltonian without it becoming significantly entangled with A , i.e., without adding dissipation at order $\mathcal{O}(1)$.

4.3.3 An example

As an illustration of our scheme, we consider a simple example wherein one seeks to indirectly control a quantum harmonic oscillator (S) by addressing only a d -level actuator (A) to which it is coupled. Existing indirect control techniques addressing this problem rely crucially on d and/or the nature of the system-actuator coupling. For instance, [103] requires a Jaynes-Cummings (JC) interaction with $d = 2$, [86] requires a JC-like coupling with $d = 3$, and [52] requires switching between two distinct interaction Hamiltonians. Our scheme, in contrast, is model independent. For illustration, however, we pick $d = 2$, the case considered in Example 4.2.

Example 4.2 Revisited: Our Indirect Control Scheme. Suppose that S and A evolve according to

$$H = \hbar\nu a^\dagger a + \frac{\hbar\omega}{2}\sigma_z + \hbar g X \otimes (\vec{n} \cdot \vec{\sigma}). \quad (4.25)$$

As in Section 4.1.1, we will not explicitly write the effect of a control field on A . Instead, we will simply assume that the actuator can be quickly and repeatedly reinitialized in a desired state, without explicitly describing the mechanism for doing so. In practice, this reinitialization could occur dynamically (e.g., through a combination of relaxation and coherent steering), through a measurement followed by a feedback pulse, or through other methods. For the sake of illustration though, we will assume the reinitialization to occur instantaneously, and S - A to be closed.

A direct application of Eq. (4.20) yields an effective Hamiltonian

$$H_{\text{eff}} = \hbar\nu a^\dagger a + \hbar g \langle \vec{n} \cdot \vec{\sigma} \rangle X, \quad (4.26)$$

which depends on ρ_A through the expectation value $\langle \vec{n} \cdot \vec{\sigma} \rangle = \text{tr}[(\vec{n} \cdot \vec{\sigma})\rho_A]$. Notice the similarity between the previous equation and Eq. (4.1): In fact, we see that choosing states $\{\rho_A^{(j)}\}$ so as to vary $\langle \vec{n} \cdot \vec{\sigma} \rangle$ in time is equivalent to choosing $V(t)$ in Example 4.1. That is, our scheme maps the indirect control problem in Example 4.2 to the direct control problem in Example 4.1.

It follows from Lloyd's result in [69] (see also [70]) that any Hamiltonian of the form

$$H = c_1 a^\dagger a + c_2 X + c_3 P, \quad (4.27)$$

where $P = (a - a^\dagger)/2i$, can be simulated on S by choosing a suitable sequence $\{\rho_A^{(j)}\}$.

In implementations, the accuracy with which one can enact evolution by H_{eff} on S through frequent resets of A will be a crucial figure of merit for this scheme. To quantify this accuracy, we consider an initial system state $\rho_S(0)$ and evolve it numerically for a time t according to the full bipartite Hamiltonian in (4.25). We then compute the fidelity F as a function of t , between the resulting reduced system state and the time-evolved state $e^{-itH_{\text{eff}}/\hbar}\rho_S(0)e^{itH_{\text{eff}}/\hbar}$ that we wish to obtain. This fidelity F is shown in Fig. 4.3 for three different rates $f = n/t$ at which the actuator is reset. (For simplicity, we suppose that the actuator is repeatedly reset to a single ρ_A here.) The technical details of this simulation are further discussed in Appendix C.

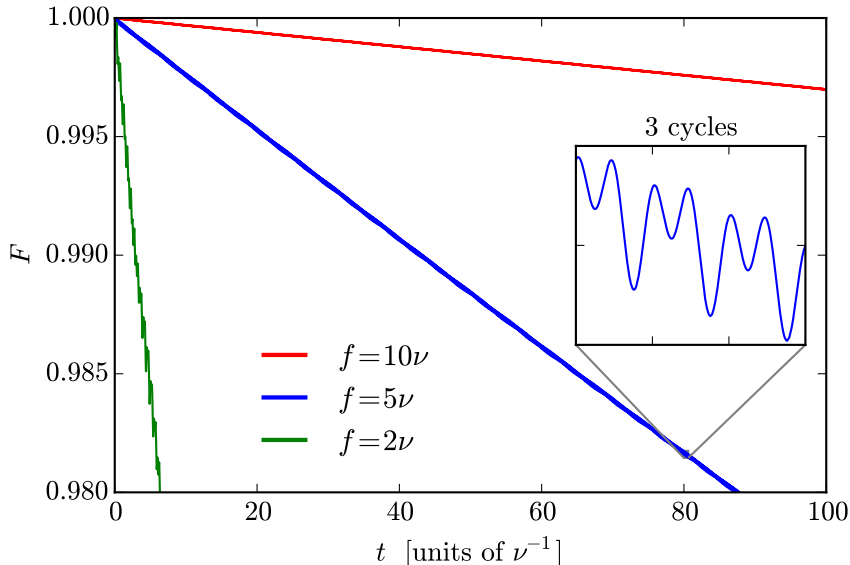


Figure 4.3: Deviation between H_{eff} and full S - A evolution where A is repeatedly reset to the state $\rho_A = (I + \sigma_x)/2$. Shown is the fidelity $F(t) = \sqrt{\langle \psi(t) | \rho_S(t) | \psi(t) \rangle}$ between $|\psi(t)\rangle = \exp(-itH_{\text{eff}}/\hbar)|\alpha\rangle$ and $\rho_S(t)$, the reduced state of S under evolution by (4.25), for three different resetting rates f . For illustration we suppose that the system starts in the coherent state $\rho_S(0) = |\alpha\rangle\langle\alpha|$ with $\alpha = (1 + i)/\sqrt{2}$, we set $\nu = \omega$, $\vec{n} = (1, 0, 0)$, and choose the switching function as $g(\tau/\delta t) = 2\nu \sin^2(\pi\tau/\delta t)$. Note for comparison that the fidelity between $|\psi(t)\rangle$ and $|\xi(t)\rangle = \exp(-itH_S/\hbar)|\alpha\rangle$, the system state time-evolved under $H_S = \hbar\nu a^\dagger a$, quickly drops to $F \sim 0.5$ over the timescale shown. This figure was made using QuTiP [54].

4.4 Error Analysis

In this section we analyse the main sources of error in our scheme, whose effects are apparent in Fig. 4.3. We define error as being a deviation between the actual reduced dynamics of the system, and that generated by $\Phi_1 = -\frac{i}{\hbar}[H_{\text{eff}}, \cdot] + \mathcal{D}_S$, which we seek to implement. In the absence of such error, the curves in Fig. 4.3 would simply be straight lines with a value of $F = 1$ for all t . (Recall that for simplicity we took $\mathcal{D}_S = 0$ to produce Fig. 4.3.) Instead, we observe two qualitatively distinct types of error: (i) a slowly growing deviation from $F = 1$ with increasing t (apparent in the main panel), and (ii) fast “wiggles” on these otherwise slowly varying curves (shown in the zoomed inset).

- Type (i) error, which we call *truncation error*, arises because S and A get slightly entangled during cycles of a finite duration. Every time A gets reset, some information is lost about S , and the system's purity is irreversibly reduced. Over time, this introduces an extra component into the system's dynamics which is not described by Φ_1 [or equivalently, by $\Omega_0(t) = \exp(\Phi_1 t)$]. Thus, truncation error becomes important on long timescales.
- Type (ii) error, which we call *stroboscopic error*, also arises from a finite reset rate f ; however, it is important only on comparatively short timescales. When f is finite, our scheme approximates smooth evolution by $\Phi_1 = -\frac{i}{\hbar}[H_{\text{eff}}, \cdot] + \mathcal{D}_S$ using discrete nonunitary kicks from A , which can have complex effects on S . Our asymptotic analysis has been focused on the total effect of each kick, considered as a lumped, discrete effect. However, the system can display complicated nonunitary (and non-Markovian) dynamics while it evolves together with A during a cycle of finite duration. These mid-cycle effects are not described by H_{eff} and \mathcal{D}_S [nor, more generally, by $\Omega_1(t), \Omega_2(t), \dots$]. Stroboscopic error, then, is the temporary deviation during each cycle between the true reduced dynamics of S and the smooth path described by Eq. (4.8). Because this type of error vanishes at the end of every cycle, it does not accumulate with t , and hence is primarily important over short timescales [of order $\mathcal{O}(\delta t)$, as opposed to $\mathcal{O}(t)$].

We now analyse both types of errors in more detail, and show how both truncation error and stroboscopic error vanish as the cycle duration goes to zero. For simplicity, we consider the case where A is repeatedly reset to a single state ρ_A .

4.4.1 Truncation error

The dynamics we wish to implement on S , generated by $\Phi_1 = -\frac{i}{\hbar}[H_{\text{eff}}, \cdot] + \mathcal{D}_S$, is completely encoded in the $\Omega_0(t)$ term of Eq. (4.8). However, higher-order terms in the effective system dynamics, while they are subdominant, are non-zero when $f < \infty$. Truncation error arises from truncating (4.8) to leading order and neglecting the $\Omega_1(t), \Omega_2(t), \dots$ terms.

To characterize truncation error, one must solve for $\Omega_1(t), \Omega_2(t), \dots$ in terms of the known superoperators Φ_1, Φ_2, \dots , whose forms are given by Eq. (4.10). We will do this by adapting the method developed in [10] (Section 4), and give an expression for $\Omega_1(t)$, the dominant (i.e., leading order) source of dissipative error.

Consider the function

$$v(\tau) := \Phi(\tau t/n)^n \Omega_0[(1 - \tau)t], \quad (4.28)$$

chosen so that $v(1) = \Phi(t/n)^n$ and $v(0) = \Omega_0(t)$. Observe that with this definition of v we have

$$\int_0^1 d\tau v'(\tau) = \frac{1}{n}\Omega_1(t) + \frac{1}{n^2}\Omega_2(t) + \dots \quad (4.29)$$

Thus, to compute $\Omega_j(t)$ in terms of $\{\Phi_k\}$ one simply has to expand $v'(\tau)$ in powers of $1/n$ and match powers n on either side of Eq. (4.29). Proceeding in this way, we have

$$v'(\tau) = \left\{ \left[\frac{d}{d\tau} \Phi(\tau t/n)^n \right] - t \Phi(\tau t/n)^n \Phi_1 \right\} e^{(1-\tau)t\Phi_1}, \quad (4.30)$$

where we have used that $\Omega_0(t) = e^{\Phi_1 t}$ from (4.13). Since $\Phi(x)$ does not generally commute with $\Phi'(x)$,

$$\frac{d}{dx} \Phi(x)^n \neq n \Phi(x)^{n-1} \Phi'(x). \quad (4.31)$$

Instead, one can easily show (see [14]) that

$$\frac{d}{d\tau} \Phi(\tau t/n)^n = t \int_0^1 d\lambda \Lambda_\lambda(\tau t/n)^{n-1} [\Phi'(\tau t/n)], \quad (4.32)$$

where we define

$$\Lambda_\lambda(\tau t/n) \cdot := \Phi(\tau t/n) - \lambda [\Phi(\tau t/n), \cdot], \quad (4.33)$$

a map on the set of superoperators for S . (In other words, for a given λ , Λ_λ is a super-operator-valued map. For any value of λ and $\tau t/n$, it transforms a superoperator on S into a different superoperator on S .) To simplify the notation, we will leave the dependence of Λ_λ on $\tau t/n$ implicit whenever possible. In other words, we will write $\Lambda_\lambda X$, for a superoperator X , to mean $\Lambda_\lambda(\tau t/n)X$.

In the same way that one arrives at Eq. (4.32) (see [14]), one can express the $\Phi(\tau t/n)^n \Phi_1$ term in $v'(\tau)$ as

$$\Phi(\tau t/n)^n \Phi_1 = \int_0^1 d\lambda \left\{ \Lambda_\lambda \Phi_1 + n(1-\lambda) \Lambda_\lambda^{n-1} [\Phi(\tau t/n), \Phi_1] \right\}. \quad (4.34)$$

It may appear as though we have needlessly complicated an otherwise-simple expression. However, (4.34) will allow us to straightforwardly expand $v'(\tau)$ in powers of $1/n$ and to

solve for $\Omega_1(t)$. Substituting Eqs. (4.32) and (4.34) into (4.30), we have

$$\begin{aligned}
v'(\tau) &= t \int_0^1 d\lambda \left(\Lambda_\lambda^{n-1} \left\{ \Phi'(\tau t/n) - \Lambda_\lambda \Phi_1 - n(1-\lambda) [\Phi(\tau t/n), \Phi_1] \right\} \right) e^{(1-\tau)t\Phi_1} \quad (4.35) \\
&= t \int_0^1 d\lambda \left\{ \left(\exp[\tau t \Lambda'_\lambda(0)] + \mathcal{O}(1/n) \right) \left[\frac{\tau t}{n} (2\Phi_2 - \Phi_1^2 \right. \right. \\
&\quad \left. \left. + \tau t(1-\lambda) [\Phi_1, \Phi_2] \right) + \mathcal{O}(1/n^2) \right] \right\} e^{(1-\tau)t\Phi_1} \\
&= \frac{t^2 \tau}{n} \int_0^1 d\lambda \left\{ e^{\tau t (\Phi_1 - \lambda [\Phi_1, \cdot])} \left[2\Phi_2 - \Phi_1^2 + \tau t(1-\lambda) [\Phi_1, \Phi_2] \right] \right\} e^{(1-\tau)t\Phi_1} + \mathcal{O}(1/n^2) \\
&= \frac{t^2 \tau}{n} \int_0^1 d\lambda e^{(1-\lambda)\tau t \Phi_1} \left(2\Phi_2 - \Phi_1^2 + \tau t(1-\lambda) [\Phi_1, \Phi_2] \right) e^{-(1-\lambda)\tau t \Phi_1} e^{\Phi_1 t} + \mathcal{O}(1/n^2) \\
&= \frac{t^2}{n} \left[e^{\tau t \Phi_1} \left(\Phi_2 - \frac{1}{2} \Phi_1^2 \right) e^{(1-\tau)t\Phi_1} \right] + \mathcal{O}(1/n^2),
\end{aligned}$$

where we have used Chernoff's theorem to expand $\Lambda_\lambda(\tau t/n)^{n-1}$ in powers of $1/n$ in the second line, in the same way that we used it to find $\Phi(t/n)^n = e^{\Phi_1 t} + \mathcal{O}(1/n)$ above. Integrating this expression for $v'(\tau)$ over $\tau \in [0, 1]$ and inserting the result into Eq. (4.29), we have

$$\frac{t^2}{n} \int_0^1 d\tau e^{\tau t \Phi_1} \left(\Phi_2 - \frac{1}{2} \Phi_1^2 \right) e^{(1-\tau)t\Phi_1} + \mathcal{O}(1/n^2) = \frac{1}{n} \Omega_1(t) + \frac{1}{n^2} \Omega_2(t) + \dots \quad (4.36)$$

Matching powers of n on both sides, we finally arrive at an expression for the next-to-leading order system propagator:

$$\frac{1}{n} \Omega_1(t) = \frac{t^2}{n} \int_0^1 d\tau e^{\tau t \Phi_1} \left(\Phi_2 - \frac{1}{2} \Phi_1^2 \right) e^{(1-\tau)t\Phi_1}. \quad (4.37)$$

Recall that $\{\Phi_j\}$ are known superoperators defined in (4.10). It is straightforward—albeit tedious—to find the form of higher-order $\Omega_j(t)$'s using this method. We will present an alternative method of performing this calculation in Chapter 5 using effective Liouvillians, which we will use to find $\Omega_2(t)$.

For our present purposes, the key part of this result is that Eq. (4.37) scales as $\mathcal{O}(t/f)$, where $f = n/t$ is the number of actuator resets per unit time. [This statement is readily formalized by noting that the induced trace norm of the integral in (4.37) is independent of t . Note that orders of dimensionful quantities are always to be understood with respect to \mathcal{L} .] This t/f scaling is apparent in Fig. 4.3, where the reset rates considered are sufficiently high that $\Omega_1(t)$ is the dominant source of truncation error. [That is, the $\mathcal{O}(1/n^2)$ terms are

highly suppressed.] In particular, observe that for each f plotted, the deviation between the reduced dynamics and the H_{eff} -generated trajectory [corresponding to $\Omega_0(t)$, the leading-order term in $1/n$] is nearly linear in t . Furthermore, the slope of the lines scale inversely with f .

4.4.2 Stroboscopic error

Let us now consider stroboscopic error. Physically, it only makes sense to apply the map $\Phi(\delta t)$ to $\rho_S(0)$ an integer number of times—the system’s state in the middle of a cycle, for instance, is *not* given by applying $\Phi(\delta t)^{1/2}$ to its initial state. However, if the cycles are short, the system’s actual evolution and the one predicted by taking fractional powers of $\Phi(\delta t)$ do not have time to diverge significantly. This temporary deviation lies at the heart of stroboscopic error. When analysing Eq. (4.8), we’ve implicitly assumed that n can grow continuously in time and take non-integer values. (This is because we’ve treated t as a steadily-growing quantity, and enforced that $t = n \delta t$ for a fixed cycle duration δt .) In other words, our description of the effective system dynamics in terms of $\Omega_0(t), \Omega_1(t), \dots$ is coarse-grained in time, and averages over the details of each cycle.

For the purposes of illustration, we will analyse stroboscopic error in the case where S - A evolves unitarily between resets. We will expand upon this preliminary analysis in Chapter 5.

One can quantify stroboscopic error by comparing the desired evolution by H_{eff} with the system’s reduced dynamics between successive resets of the actuator. We use a truncated Dyson series to perform this comparison: If $\rho_S(t_n)$ is the system’s state after cycle n , then during cycle $n + 1$, evolution by H_{eff} would give

$$\rho_S^{(\text{eff})}(t_n + \tau) = \rho_S(t_n) - \frac{i\tau}{\hbar} [H_{\text{eff}}, \rho_S(t_n)] + \mathcal{O}(\tau^2), \quad (4.38)$$

for $0 < \tau < \delta t$. When the cycles are short, i.e., when $\tau < \delta t \ll 1$ in units set by the largest characteristic frequency of $H(\tau)$, the $\mathcal{O}(\tau^2)$ terms in the Dyson series will be subdominant, and so we work only to first order in τ here.

Eq. (4.38) describes the dynamics our scheme seeks to implement. However, the actual full evolution of S between successive actuator resets is computed by evolving S - A according to $H(\tau)$ and then tracing out the actuator:

$$\rho_S^{(\text{full})}(t_n + \tau) = \rho_S(t_n) - \frac{i}{\hbar} \left[\int_0^\tau d\tau' H(\tau'), \rho_S(t_n) \otimes \rho_A \right] + \mathcal{O}(\tau^2). \quad (4.39)$$

Concretely, stroboscopic error is described by the difference between Eqs. (4.38) and (4.39):

$$\rho_S^{(\text{eff})}(t_n + \tau) - \rho_S^{(\text{full})}(t_n + \tau) = -\frac{i\tau}{\hbar} \left\{ \bar{g} - \frac{\delta t}{\tau} \int_0^{\tau/\delta t} d\zeta g(\zeta) \right\} [\text{tr}_A(H_{SA}\rho_A), \rho_S(t_n)] + \mathcal{O}(\tau^2). \quad (4.40)$$

The braced term in Eq. (4.40) is bounded above in magnitude by $2g_{\text{max}}(\delta t - \tau)/\tau$, where g_{max} is the largest coupling strength attained in each cycle. (Thus, stroboscopic error is reduced when the system-actuator coupling is weak.) The commutator in the previous equation, in contrast, can vary arbitrarily with t_n , depending on the nature of $H(t)$. However, it is always suppressed by a prefactor of $\delta t - \tau$, and so (4.40) generically scales as $\mathcal{O}(\delta t - \tau)$, which is upper bounded by $\mathcal{O}(\delta t)$. In terms of the actuator reset frequency then, stroboscopic error scales as $\mathcal{O}(1/f)$.

Unlike truncation error, which accumulates with t , stroboscopic error vanishes with each actuator reset. Thus, while the former type is reduced by implementing H_{eff} for relatively short durations t , the latter can be sidestepped entirely by choosing f and t to give an integer number of cycles. In general, both types of error can be suppressed arbitrarily by choosing an f that is large as compared to the characteristic frequencies of H .

4.5 Discussion

We begin by noting that the analysis in this chapter involved certain idealizations which were convenient but not strictly necessary. For instance, we assumed that the actuator was reset (or more generally, reinitialized) instantaneously. However, this need not be the case. The reinitialization could instead be accomplished quickly (as compared to the natural timescales of S - A) by measuring A and then applying a strong and rapid pulse to it, conditioned on the measurement outcome, in order to prepare a desired state $\rho_A^{(j)}$. Alternatively, A could be reset gradually purely through dynamical effects. For instance, strong dissipation could return it to an equilibrium state (e.g., a thermal state) throughout each cycle. (This resembles a scenario described in [109], and the resulting system behaviour is similar to our scheme. Accordingly, future efforts to characterize the effects of imperfect resetting in our scheme will likely incorporate techniques from [108, 109] into our current approach.) This dynamical reset could be used in conjunction with appropriate pulses to prepare different $\rho_A^{(j)}$'s with each cycle. Also, we note that Chernoff's theorem—which gives the leading-order system dynamics in the high f regime—can be generalized to describe cycles of non-uniform duration. Specifically, when n actuator resets are performed in a time t , the system's evolution will be well described by H_{eff} (or

more generally, by Φ_1) when the longest time between actuator resets is sufficiently short [92, 93].

The indirect control scheme presented here has three main features:

Feature 1. To leading order, it separates the timescales on which a system can be controlled from the timescales on which a system experiences decoherence. This feature is manifest in Eq. (4.23), where we see that to order $\mathcal{O}(1)$ the system’s Hamiltonian is non-trivially modified by A , but its dissipator is not.

Feature 2. It allows one to map the potentially intractable problem of indirect quantum control to the simpler one of direct control. Instead of finding a driving pulse that will directly produce a desired unitary on the system, one instead finds the sequence of actuator states $\{\rho_A^{(j)}\}$ that will have the same effect. While physically these two approaches seem very different, they are mathematically equivalent.

Feature 3. It makes (almost) no assumptions on the nature of S and A , nor on the coupling between them. [The one caveat is that H_S and $\text{tr}(H_{SA}\rho_A)$ cannot be related by a special commutation relation for all ρ_A which causes the algebra they generate through commutation to not include all potential Hamiltonians on the system [69], as in the dispersive Jaynes-Cummings Hamiltonian, for instance.]

We emphasize, however, that the scheme’s performance depends crucially on one’s ability to implement rapid cycles. In particular, Feature 1 is an interesting property of the leading order system dynamics, in powers of $1/n$, or equivalently, in the inverse reinitialization frequency, f^{-1} . If f is not sufficiently large (in units set by \mathcal{L}), higher-order effects from $\Omega_1(t), \Omega_2(t), \dots$ can potentially nullify the favourable features in the leading-order dynamics.

There remain several aspects of this scheme which require further analysis—especially parts pertaining to experimental implementations. For instance, we have required (pessimistically) that the reinitialization frequency f be large compared to all characteristic frequencies of S - A . It would be useful to refine this requirement in terms of the characteristic frequencies of H_S , H_A , and H_{SA} separately. For example, the free dynamics of A do not contribute to H_{eff} , which hints that it may only be necessary for f to be small compared to the frequencies of H_S and H_{SA} . This point could be important in practice: taking the nuclear spin in an NV centre as S and the electron spin as A , the characteristic frequency of H_A is on the order of 1 GHz, while those of H_S and H_{SA} are on the order of 1 MHz [25]. Since A in this system can be controlled on timescales of a few nanoseconds [1] (i.e.,

rapidly compared to H_S and H_{SA} , but not compared to H_A), a more precise bound for f will determine whether our scheme is well-suited for this system, and for several others.

Another natural question is: how quickly can one vary the actuator states $\rho_A^{(j)}$ with each cycle to accurately implement a time-varying H_{eff} ? We argued in this chapter that the variation in these states needed to be slow compared to δt , the cycle duration. Given experimental constraints on δt , however, exactly how slowly one must go to maintain tolerably low error has yet to be determined. Another area meriting further analysis are the effects of imperfect actuator reinitialization, especially if this is to be accomplished dynamically, in an open-loop fashion (i.e., without feedback).

There also remain a number of outstanding questions regarding potential applications of this scheme. For instance, could it be used to steer S adiabatically? On one hand, one could imagine choosing $\{\rho_A^{(j)}\}$ so as to adiabatically change H_{eff} . This could hypothetically be used, for instance, to prepare eigenstates of H_{eff} by starting in an eigenstate of H_S . (In the case of Example 4.2, the eigenstates of H_{eff} are *photon-added states*, which can be highly non-classical [111]). On the other hand, our scheme relies on rapidly repeated kicks to the system, which seem inherently non-adiabatic. The interplay between rapid kicks and an adiabatically varying H_{eff} requires further analysis.

Finally, while this chapter has been concerned with coherent control, we wish to point out possible extensions of our scheme which could also provide indirect dissipative control (e.g., for Lindblad simulation). One way to do this would be to measure the actuator instead of simply resetting it, and conditioning future cycles on the result; this resembles the approach proposed by Lloyd and Viola in Ref. [72] to simulate arbitrary open dynamics. Another approach, which will form the basis of the next chapter, would be to exploit higher order effects [coming from $\Omega_1(t), \Omega_2(t), \dots$] in the system's reduced dynamics to not only implement an effective Hamiltonian on S , but to engineer an effective Liouvillian.

Chapter 5

Indirect Quantum Control: Dissipative Control

In this chapter we present a subset of the material published in [40], and discuss potential extensions of the control scheme introduced in Chapter 4.

5.1 Motivation

The scheme presented in the previous chapter was motivated by the need for rapid coherent control of quantum systems. In particular, indirect control provides a way to coherently steer systems quickly as compared to the timescales on which they experience significant dissipation. Dissipation, when it arises due to of a noisy and uncontrolled environment, usually represents a hindrance to quantum technologies, as it suppresses the manifestly quantum phenomena that give these technologies an advantage over their classical counterparts. However, dissipation is not always undesirable. In fact, a purposefully-engineered dissipative component in a system's dynamics can, in principle, be used as the basis for state preparation, quantum simulation, and even universal quantum computing. (See [110] for an overview of these applications.)

There exist a number of approaches for implementing controlled dissipation in quantum systems. Ref. [72], for instances, proposes a digital approach, where the usual circuit model for unitary quantum computation is enhanced by feeding the outcomes of measurements on ancillas back into the circuit. In contrast, Ref. [110] (building upon earlier results in

[108, 109] which were discussed in Section 4.3.1) proposes an analogue approach which involves engineering a system’s effective environment in order to simulate a desired Lindblad dynamics.

In this chapter, we discuss a potential extension of the scheme from Chapter 4 and develop some of the theoretical tools required for such an extension. Concretely, just as we previously used frequent reinitialization of an actuator to effectively modify a system’s Hamiltonian, we envisage modifying also the dissipative part of the system’s effective dynamics with this approach. Doing so would require one to exploit higher-order terms in the system’s effective dynamics. Recall from the previous chapter that in our scheme the system’s Hamiltonian was modified by the actuator whereas the dissipative part of its dynamics remained unchanged to leading order. At next-to-leading order, however, both parts of the effective system dynamics are generically affected by the actuator. Thus, instead of utilizing only the leading-order part of the system’s effective dynamics and treating higher-order effects as error (which we called “truncation error” in the previous chapter), we present here a preliminary analysis of these higher order effects, and discuss their potential for indirectly implementing arbitrary Lindblad dynamics.

5.2 An Effective System Liouvillian

We found in Chapter 4 that the system’s reduced dynamics under frequent actuator resets was described by

$$\rho_S(t) = \underbrace{e^{\Phi_1 t}}_{\Omega_0(t)} \rho_S(0) + \mathcal{O}(1/n). \quad (5.1)$$

In this chapter, we will often expand such expressions not in powers of $1/n$, where n is the number of cycles in $[0, t]$, but rather, in powers of the cycle duration δt . While $1/n$ is a dimensionless parameter (in contrast with δt), it varies with time as $n = t/\delta t$, which makes for messy time-derivatives. For the present analysis, it will be more convenient to expand in powers of the fixed cycle duration δt , which is a constant. Note that this is simply a technical detail, as series expansions in $1/n$ and δt are equivalent in the present context. Note also that we will understand expansions in δt to be in units set by the natural dynamics of S - A .

In terms of δt , Eq. (5.1) can be re-written as

$$\rho_S(t) = e^{\Phi_1 t} \rho_S(0) + \mathcal{O}(\delta t), \quad (5.2)$$

from which it follows that

$$\frac{d}{dt}\rho_S(t) = \Phi_1\rho_S(t) + \mathcal{O}(\delta t). \quad (5.3)$$

In other words, Φ_1 plays the role of an effective Liouvillian describing the system's leading-order dynamics. In the previous chapter, we sought to implement this effective dynamics, and treated any deviation from the Φ_1 -generated evolution as error. Here, in contrast, we will seek to describe the effective dynamics of S beyond order $\mathcal{O}(1)$. In particular, for a given δt we will seek an effective Liouvillian for the system, \mathcal{L}_{eff} , which we will expand in powers of δt as

$$\mathcal{L}_{\text{eff}} = \mathcal{L}_0 + \delta t\mathcal{L}_1 + \delta t^2\mathcal{L}_2 + \dots \quad (5.4)$$

The main results in Chapter 4 revolved around \mathcal{L}_0 and its properties. Upon comparing the previous equation with (5.3), we identify $\mathcal{L}_0 = \Phi_1$. What do $\mathcal{L}_1, \mathcal{L}_2, \dots$ look like?

As we discussed in Section 4.4.2, only integer powers of the map $\Phi(\delta t)$ give an exact description of the system's dynamics. Non-integer powers, on the other hand, only give an approximate description, which includes stroboscopic error. Concretely:

$$\rho_S(\delta t) = \Phi(\delta t)\rho_S(0), \quad (5.5)$$

and likewise for integer multiples of δt , but

$$\rho_S(\delta t/2) \approx \Phi(\delta t)^{1/2}\rho_S(0), \quad (5.6)$$

and likewise for other fractional multiples of δt . The full expression for \mathcal{L}_{eff} , to all powers in δt , will contain the same information as the superoperators $\Omega_0(t), \Omega_1(t), \dots$ which form the effective system propagator [see Eq. (4.8)]. Like these $\Omega_j(t)$'s, however, \mathcal{L}_{eff} will not account for mid-cycle effects, but will instead also give a description of the system dynamics that is coarse-grained in time and that smooths out these effects.

In order to derive this effective Liouvillian, we will suppose, as a mathematical tool, that the system's dynamics is described by continuously-growing powers of $\Phi(\delta t)$. This amounts to accepting Eq. (5.6) as a reasonably good approximation. More precisely, we will make the approximation that

$$\rho_S(t) \approx \Phi(\delta t)^{t/\delta t}\rho_S(0), \quad (5.7)$$

for all values of $t/\delta t$, even though exact equality is only achieved for $t/\delta t \in \mathbb{Z}$. As per our discussion of stroboscopic error in the previous chapter, we expect this approximation to become arbitrarily good when δt is taken to be sufficiently small. We will discuss the stroboscopic error resulting from this approximation more thoroughly in Section 5.4.

Building upon the previous equation, we have that

$$\begin{aligned}\rho_S(t + \epsilon) - \rho_S(t) &\approx \left[\Phi(\delta t)^{(t+\epsilon)/\delta} - \Phi(\delta t)^{t/\delta t} \right] \rho_S(0) \\ &= \left[\Phi(\delta t)^{\epsilon/\delta t} - I \right] \underbrace{\Phi(\delta t)^{t/\delta t} \rho_S(0)}_{\rho_S(t)}.\end{aligned}\quad (5.8)$$

We then arrive at a first-order differential equation for the effective system dynamics:

$$\frac{d}{dt} \rho_S(t) \approx \left[\frac{1}{\delta t} \lim_{h \rightarrow 0} \frac{\Phi(\delta t)^h - I}{h} \right] \rho_S(t) = \left[\frac{1}{\delta t} \frac{d}{dx} \Big|_{x=0} \Phi(\delta t)^x \right] \rho_S(t). \quad (5.9)$$

One can show that

$$\frac{d}{dx} \Big|_{x=0} \Phi(\delta t)^x = \ln \Phi(\delta t), \quad (5.10)$$

where we have chosen the complex branch by requiring that the spectrum of \mathcal{L}_{eff} match that of $-\frac{1}{i\hbar}[H_S, \cdot]$ when the S - A coupling is taken to vanish. Therefore:

$$\mathcal{L}_{\text{eff}} = \frac{1}{\delta t} \ln \Phi(\delta t). \quad (5.11)$$

To arrive at an expression for \mathcal{L}_{eff} in powers of δt , one need only substitute Eq. (4.9) into the Taylor expansion for $\ln \Phi(\delta t)$. Concretely,

$$\begin{aligned}\mathcal{L}_{\text{eff}} &= \frac{1}{\delta t} \sum_{k=1}^{\infty} \frac{(-1)^{k+1}}{k} \left(\Phi(\delta t) - I \right)^k \\ &= \frac{1}{\delta t} \sum_{k=1}^{\infty} \frac{(-1)^{k+1}}{k} \left(\delta t \Phi_1 + \delta t^2 \Phi_2 + \delta t^3 \Phi_3 + \dots \right)^k \\ &= \underbrace{\Phi_1}_{\mathcal{L}_0} + \delta t \underbrace{\left(\Phi_2 - \frac{1}{2} \Phi_1^2 \right)}_{\mathcal{L}_1} + \delta t^2 \underbrace{\left(\Phi_3 - \frac{1}{2} \{ \Phi_1, \Phi_2 \} + \frac{1}{3} \Phi_1^3 \right)}_{\mathcal{L}_2} + \dots,\end{aligned}\quad (5.12)$$

where the superoperators Φ_j are defined in Eq. (4.10). Notice that, as expected, Φ_1 is the leading-order component of the system's effective Liouvillian. Higher-order terms in \mathcal{L}_{eff} can easily be found by gathering appropriate powers of δt in the second line of the previous expression. Note that the procedure for finding \mathcal{L}_k in terms of $\{\Phi_j\}$ is similar to that of converting between a Dyson and a Magnus series (see, e.g., [3]).

An expression for \mathcal{L}_{eff} to order $\mathcal{O}(\delta t)$ is expressed in Lindblad form in Ref. [40]. The expression is lengthy, but the key point is that \mathcal{L}_1 adds corrections to both the Hamiltonian and dissipative parts of the system's effective dynamics, both of which depend on ρ_A .

5.3 Higher-Order Propagators

Our expression for \mathcal{L}_{eff} can be used to find the superoperators $\Omega_0(t), \Omega_1(t), \dots$ in Eq. (4.8). We will outline a method for doing so, and show that we recover our previous expressions for $\Omega_0(t), \Omega_1(t), \dots$, which we found through an entirely different technique. Assuming that

$$\rho_S(t) = e^{\mathcal{L}_{\text{eff}}t} \rho_S(0) \quad (5.13)$$

$$= \exp \left[(\mathcal{L}_0 + \delta t \mathcal{L}_1 + \delta t^2 \mathcal{L}_2 + \dots) t \right] \rho_S(0) \quad (5.14)$$

for $t = n \delta t$, we expand the propagator $e^{\mathcal{L}_{\text{eff}}t}$ in powers of δt to find

$$\rho_S(t) = \left[e^{\mathcal{L}_0 t} + \delta t \frac{d}{d(\delta t)} \Big|_{\delta t=0} e^{\mathcal{L}_{\text{eff}}t} + \mathcal{O}(\delta t^2) \right] \rho_S(0). \quad (5.15)$$

Using now that

$$\frac{d}{dx} e^{A(x)} = \int_0^1 d\tau e^{A(x)\tau} A'(x) e^{(1-\tau)A(x)}, \quad (5.16)$$

a corollary of the Baker-Campbell-Hausdorff formula [which is non-trivial when $A(x)$ does not commute with $A'(x)$], we identify $x = \delta t$ and $A(x) = \mathcal{L}_{\text{eff}}t$. (Note that the latter expression depends on δt through \mathcal{L}_{eff}). We may then expand Eq. (5.15) as

$$\rho_S(t) = \left[\underbrace{e^{\Phi_1 t}}_{\Omega_0(t)} + \delta t \cdot t \underbrace{\int_0^1 d\tau e^{\tau t \Phi_1} \mathcal{L}_1 e^{(1-\tau)t \Phi_1}}_{\frac{\delta t}{t} \Omega_1(t)} + \mathcal{O}(\delta t^2) \right] \rho_S(0). \quad (5.17)$$

Comparing with Eq. (4.8) and noting that $\mathcal{L}_1 = \Phi_2 - \Phi_1^2/2$, we see that we have exactly recovered our expressions for $\Omega_0(t)$ and $\Omega_1(t)$ from Chapter 4 using an effective Liouvillian for the system. We can easily extend this method to find $\Omega_j(t)$ for $j \geq 2$. For instance, by computing further powers in Eq. (5.15) one quickly finds that

$$\begin{aligned} \Omega_2(t) = \frac{1}{2} \int_0^1 d\tau \int_0^1 d\nu \left\{ t^4 \tau e^{\tau \nu t \mathcal{L}_0} \mathcal{L}_1 e^{(1-\nu)\tau t \mathcal{L}_0} \mathcal{L}_1 e^{(1-\tau)t \mathcal{L}_0} \right. \\ \left. + 2t^3 e^{t\tau \mathcal{L}_0} \mathcal{L}_2 e^{t(1-\tau)\mathcal{L}_0} \right. \\ \left. + t^4 (1-\tau) e^{\tau t \mathcal{L}_0} \mathcal{L}_1 e^{t(1-\tau)\nu \mathcal{L}_0} \mathcal{L}_1 e^{(1-\nu)(1-\tau)t \mathcal{L}_0} \right\}. \end{aligned} \quad (5.18)$$

5.3.1 Numerical test

In order to verify our expressions for $\Omega_0(t)$, $\Omega_1(t)$ and $\Omega_2(t)$, we performed a numerical test for the case where both S and A are qubits which evolve unitarily according to a time-independent Hamiltonian between resets of A . We used the following algorithm to test our expression for $\Omega_j(t)$:

Repeat:

1. Pick a Hamiltonian $H \in \text{herm}(4)$ for S - A and an initial actuator state ρ_A at random.
2. Define superoperators $\Phi(t/n)$ and $\{\Phi_j\}$, using Eqs. (4.7) and (4.10), for this choice of H and ρ_A .
3. Represent density matrices of S as vectors in \mathbb{R}^4 , and correspondingly, superoperators on S as 4×4 matrices. We used the isomorphism

$$\begin{pmatrix} a & b - ic \\ b + ic & d \end{pmatrix} \leftrightarrow \begin{pmatrix} a \\ b \\ c \\ d \end{pmatrix}, \quad (5.19)$$

which has the convenient feature of mapping superoperators on S to real (as opposed to complex) matrices. If F is a superoperator on S , we will denote its matrix representation under (5.19) as $[F]$.

4. For an arbitrary t , compute

$$[\Delta_j(n)] := n^j \left([\Phi(t/n)]^n - \sum_{k=0}^{j-1} n^{-k} [\Omega_k(t)] \right) \quad (5.20)$$

for increasingly large n until convergence (under the Frobenius norm). Compare the resulting $[\Delta_j(n)]$ matrix with $[\Omega_j(t)]$.

The rationale behind this approach comes from rearranging Eq. (4.8). For illustration, we consider $j = 1$, for which we have

$$\begin{aligned} \Phi(t/n)^n &= \Omega_0(t) + \frac{1}{n}\Omega_1(t) + \frac{1}{n^2}\Omega_2(t) + \dots \\ &\quad \downarrow \\ \Omega_1(t) &= \underbrace{n[\Phi(t/n)^n - \Omega_0(t)]}_{\Delta_1(n)} - \underbrace{n\left[\frac{1}{n^2}\Omega_2(t) + \dots\right]}_{\mathcal{O}(1/n)}. \end{aligned} \quad (5.21)$$

Therefore, we expect

$$[\Delta_1(n)] = n \left([\Phi(t/n)]^n - [\Omega_0(t)] \right) \rightarrow [\Omega_1(t)] \text{ as } n \rightarrow \infty. \quad (5.22)$$

More generally, if our expressions for $\Omega_j(t)$ are correct, one would expect $[\Delta_j(n)] \rightarrow [\Omega_j(t)]$ for sufficiently large n .

For every randomly generated combination of H , ρ_A , and t , we indeed found that $[\Delta_j(t)] \rightarrow [\Omega_j(t)]$ as $n \rightarrow \infty$ under the Frobenius norm for $j = 0, 1, 2$. This finding provides substantial numerical evidence in support of our expressions for $\Omega_0(t)$, $\Omega_1(t)$, and $\Omega_2(t)$.

5.4 Stroboscopic Error at Higher Orders

If we are to purposely employ higher-order effects in the system's dynamics for indirect dissipative control, it is important that we characterize stroboscopic error to higher orders in δt . To do so, we expand upon the strategy used in Section 4.4.2. Concretely, we compare the system's true state at a time τ after the n -th actuator reset, with that predicted by \mathcal{L}_{eff} for the same time. We give the result in the form of a bound on the difference between these states, in powers of δt :

$$\|\rho_S^{(\text{full})}(t_n + \tau) - \rho_S^{(\text{eff})}(t_n + \tau)\| \leq c_1 \delta t + c_2 \delta t^2 + c_3 \delta t^3 + \dots, \quad (5.23)$$

where $\|X\|$ denotes the trace norm of an operator X , defined as $\|X\| := \text{tr} \sqrt{X^\dagger X}$. As in Section 4.4.2, we take $t_n = n \delta t$ (for some integer n), $0 < \tau < \delta t$, $\rho_S^{(\text{eff})}(t) = e^{\mathcal{L}_{\text{eff}} t} \rho_S(0)$, and $\rho_S^{(\text{full})}(t)$ to be the true state of the system at a time $t_n + \tau$ under the full S - A evolution [see Eq. (5.30)]. Note that our analysis of stroboscopic error in the previous chapter was only concerned with the $\mathcal{O}(\delta t)$ effects.

We now outline a method to solve for all coefficients $\{c_j\}$ and we give, in particular, expressions for c_1 and c_2 . We will assume for simplicity that A is reset to the same state ρ_A with every cycle. We begin with some preliminary observations.

First, we consider a generic superoperator $A(t)$ on S . Using the trace norm and the operator norm it induces throughout, we have for $0 < x < 1$ that

$$\begin{aligned} \left\| \int_0^1 dt A(t) - \frac{1}{x} \int_0^x dt A(t) \right\| &= \left\| \left(1 - \frac{1}{x}\right) \int_0^1 dt A(t) + \int_x^1 dt A(t) \right\| \\ &\leq \int_0^1 dt \|A(t)\| + \left(\frac{1}{x} - 2\right) \int_0^x dt \|A(t)\|, \end{aligned} \quad (5.24)$$

where we have used the triangle inequality. Defining the superoperator-valued function

$$G(x) := \left(2 - \frac{1}{x}\right) \int_0^x dt \|A(t)\| \quad (5.25)$$

and substituting (5.25) into the previous inequality yields

$$\left\| \int_0^1 dt A(t) - \frac{1}{x} \int_0^x dt A(t) \right\| \leq G(1) - G(x) = G'(\xi)(1-x), \quad (5.26)$$

for some $\xi \in (x, 1)$, where we have assumed $A(t)$ to be continuous in order to use the Mean Value Theorem for $\|A(t)\|$. Examining the derivative of G , we have

$$\begin{aligned} G'(\xi) &= \frac{1}{\xi^2} \int_0^\xi dt \|A(t)\| + \left(2 - \frac{1}{\xi}\right) \|A(\xi)\| \\ &\leq \frac{2}{\xi} \max_{0 < t < 1} \|A(t)\|. \end{aligned} \quad (5.27)$$

It follows that

$$\left\| \int_0^1 dt A(t) - \frac{1}{x} \int_0^x dt A(t) \right\| \leq \frac{2(1-x)}{x} \max_{0 < t < 1} \|A(t)\|. \quad (5.28)$$

To simplify later notation, we define an operator Γ which acts on superoperator-valued maps as

$$(\Gamma A)(x) := \int_0^1 dt A(t) - \frac{1}{x} \int_0^x dt A(t). \quad (5.29)$$

The left-hand side of Eq. (5.28) can now be written in the compact form $\|(\Gamma A)(x)\|$. Let us make some more preliminary observations:

- It is simple to show that if $\|\mathcal{L}\| = -\frac{i}{\hbar}[H, \cdot]$ then $\|\mathcal{L}\| \leq \frac{2}{\hbar}\|H\|$.
- Similarly, if \mathcal{L} is a superoperator on S - A and $\mathcal{L}_{\text{red}} := \text{tr}_A[\mathcal{L}(\cdot \otimes \rho_A)]$ is a superoperator on S , then $\|\mathcal{L}_{\text{red}}\| \leq \|\mathcal{L}\|$. This follows immediately from the contractivity of the partial trace under the trace norm [80].
- The operator norm induced by the trace norm is submultiplicative, i.e., $\|\mathcal{L}_1 \mathcal{L}_2\| \leq \|\mathcal{L}_1\| \|\mathcal{L}_2\|$ for superoperators \mathcal{L}_1 and \mathcal{L}_2 . This is a general property of induced norms.

We now derive the main result concerning stroboscopic error. Following Section 4.4.2, the full evolution of the system is described by

$$\rho_S^{(\text{full})}(t_n + \tau) = \text{tr}_A \left\{ \mathcal{T} e^{\int_0^\tau dt' \mathcal{L}(t')} [\rho_S(t_n) \otimes \rho_A] \right\}. \quad (5.30)$$

Expanding (5.30) in powers of τ yields

$$\begin{aligned} \rho_S^{(\text{ex})}(t_n + \tau) = & \rho_S(t_n) + \underbrace{\text{tr}_A \left\{ \int_0^\tau dt' \mathcal{L}(t') [\rho_S(t_n) \otimes \rho_A] \right\}}_{\Xi_1 \rho_S(t_n)} \\ & + \underbrace{\text{tr}_A \left\{ \int_0^\tau dt' \int_0^{t'} dt'' \mathcal{L}(t') \mathcal{L}(t'') [\rho_S(t_n) \otimes \rho_A] \right\}}_{\Xi_2 \rho_S(t_n)} + \mathcal{O}(\tau^3), \end{aligned} \quad (5.31)$$

where we define superoperators Ξ_j as indicated in the expression above. On the other hand, the \mathcal{L}_{eff} -generated dynamics gives

$$\rho_S^{(\text{eff})}(t_n + \tau) = e^{\mathcal{L}_{\text{eff}}\tau} \rho_S(t_n) = \left[I + \tau \mathcal{L}_{\text{eff}} + \frac{\tau^2}{2} \mathcal{L}_{\text{eff}}^2 + \mathcal{O}(\tau^3) \right] \rho_S(t_n). \quad (5.32)$$

To characterize the magnitude of stroboscopic error, we subtract Eqs. (5.31) and (5.32) and collect powers of δt and τ . In particular, we extract the τ and δt -dependence from all terms in the form of a prefactor $\delta t^\alpha \tau^\beta$, and collect terms having the same value of $\alpha + \beta$. The physical justification for this approach comes from the fact that we seek here to describe dynamics on timescales of order $\mathcal{O}(\delta t)$, and so τ and δt must be comparable in magnitude. Concretely, we have that

$$\begin{aligned} & \rho_S^{(\text{ex})}(t_n + \tau) - \rho_S^{(\text{eff})}(t_n + \tau) \\ & = \left\{ [I + \Xi_1 + \Xi_2 + \dots] - [I + \tau \mathcal{L}_0 + (\tau \delta t \mathcal{L}_1 + \frac{\tau^2}{2} \mathcal{L}_0^2) + \dots] \right\} \rho_S(t_n). \end{aligned} \quad (5.33)$$

We characterize here the stroboscopic error to order $\mathcal{O}(\delta t^2)$. While lengthy, it is straightforward to extend this procedure to higher orders.

Inserting into the expression above the decomposition of \mathcal{L} into system, ancilla and interaction terms [see Eq. (4.5)], one finds that the leading-order component of (5.33) goes as

$$\Xi_1 - \tau \mathcal{L}_0 = -\tau \text{tr}_A \left\{ \left[(\Gamma \mathcal{L}_{SA})(\tau/\delta t) \right] (\cdot \otimes \rho_A) \right\}. \quad (5.34)$$

Using Eq. (5.28) and our other preliminary observations, we bound the norm of Eq. (5.34) as

$$\|\Xi_1 - \tau \mathcal{L}_0\| \leq 2(\delta t - \tau) \|\mathcal{L}_{SA}\|_{\max}, \quad (5.35)$$

where $\|\mathcal{L}_{SA}\|_{\max} := \max_{0 < \zeta < 1} \|\mathcal{L}_{SA}(\zeta)\|$. Similarly, the sub-leading order terms in (5.33) go as

$$\begin{aligned} \Xi_2 - \tau \delta t \mathcal{L}_1 - \frac{\tau^2}{2} \mathcal{L}_0^2 &= \frac{\tau}{2} (\delta t - \tau) \left[\int_0^1 d\zeta \left\{ \mathcal{L}_S, \text{tr}_A [\mathcal{L}_{SA}(\zeta)(\cdot \otimes \rho_A)] \right\} \right. \\ &\quad \left. + \left(\int_0^1 d\zeta \text{tr}_A [\mathcal{L}_{SA}(\zeta)(\cdot \otimes \rho_A)] \right)^2 \right] \\ &\quad - \tau \delta t \text{tr}_A \left\{ [(\Gamma A)(\tau/\delta t)](\cdot \otimes \rho_A) \right\}, \end{aligned} \quad (5.36)$$

where

$$A(\zeta) = \zeta \mathcal{L}_{SA}(\zeta) (\mathcal{L}_S + \mathcal{L}_A) + [\mathcal{L}_S + \mathcal{L}_A + \mathcal{L}_{SA}(\zeta)] \int_0^\zeta d\zeta' \mathcal{L}_{SA}(\zeta') \quad (5.37)$$

and $\{\cdot, \cdot\}$ denotes an anti-commutator. Thus, the sub-leading order contribution to stroboscopic error is bounded in norm as

$$\begin{aligned} \|\Xi_2 - \tau \delta t \mathcal{L}_1 + \frac{\tau^2}{2} \mathcal{L}_0^2\| &\leq \frac{\delta t - \tau}{2} \|\mathcal{L}_{SA}\|_{\max} \\ &\times \left\{ \tau \left(2\|\mathcal{L}_S\| + \|\mathcal{L}_{SA}\|_{\max} \right) + 4\delta t \left(2\|\mathcal{L}_S\| + 2\|\mathcal{L}_A\| + \|\mathcal{L}_{SA}\|_{\max} \right) \right\}. \end{aligned} \quad (5.38)$$

Maximizing over $\tau \in (0, \delta t)$ in Eqs. (5.35) and (5.38), one finds coefficients

$$c_1 = 2\|\mathcal{L}_{SA}\|_{\max}, \quad (5.39)$$

$$c_2 = \|\mathcal{L}_{SA}\|_{\max} \left(\frac{17}{4} \|\mathcal{L}_S\| + 4\|\mathcal{L}_A\| + \frac{17}{8} \|\mathcal{L}_{SA}\|_{\max} \right), \quad (5.40)$$

describing the magnitude of stroboscopic error in Eq. (5.23). In the special case considered in Section 4.4.2 where S - A is closed and the only time dependence in its Hamiltonian is contained in a switching function g , these coefficients become

$$c_1 = \frac{4g_{\max}}{\hbar} \|H_{SA}\| \quad (5.41)$$

$$c_2 = \frac{g_{\max}}{\hbar^2} \|H_{SA}\| \left(17\|H_S\| + 16\|H_A\| + \frac{17g_{\max}}{2} \|H_{SA}\| \right), \quad (5.42)$$

where we have assumed all norms in the above expressions to be finite¹.

Observe that to leading order in δt , the magnitude of stroboscopic error depends linearly on the S - A coupling strength, as found in Section 4.4.2. To $\mathcal{O}(\delta t^2)$, however, stroboscopic error depends not only on the interaction Hamiltonian, but it also scales non-trivially with the free Hamiltonians of S and A . As in the previous chapter, we find stroboscopic error to vanish as the cycle duration δt becomes short.

5.5 Discussion

In this chapter we have introduced a number of tools required to extend the indirect control scheme presented in Chapter 4 to include both coherent and dissipative control. In particular, we described the effective dynamics of S under frequent resets of A to all orders using an effective Liouvillian, and we analysed the stroboscopic error associated with such a description.

Just as H_{eff} in the previous chapter depended on ρ_A , the state to which A is reinitialized, we found more generally that \mathcal{L}_{eff} depends on ρ_A , suggesting the possibility of engineering both the Hamiltonian and dissipative parts of the system’s effective dynamics. We envisage four main applications of such indirect dissipative control:

Lindblad simulation In Chapter 4, we found that one could indirectly implement a continuous family of effective Hamiltonians on S by repeatedly resetting A to an appropriate state ρ_A . Moreover, by reinitializing A in a slowly-varying sequence of states $\{\rho_A^{(j)}\}$ instead of simply resetting it, one could implement a time-dependent H_{eff} on S . This strategy extends naturally to \mathcal{L}_{eff} , which could be used to simulate a Liouvillian of interest by reinitializing A in a suitable sequence of states. This amounts to harnessing higher-order effects in the system’s effective dynamics—effects which were treated as truncation error in the previous chapter, where the goal was only to implement H_{eff} (or rather, \mathcal{L}_0).

Decoupling An immediate application of Lindblad simulation would be to decouple the system from its environment (at least partially). This could be achieved by choosing an appropriate sequence $\{\rho_A^{(j)}\}$ so as to cancel, or at least attenuate, the terms in

¹In cases where the normed difference in Eq. (5.23) does not provide an adequate description of deviation between the full and \mathcal{L}_{eff} -generated dynamics (e.g., in infinite-dimensional systems, such as quantum fields, where the relevant norms may be undefined), one could repeat the above analysis without the use of norms, following Section 4.4.2

\mathcal{L}_{eff} arising due to system-environment coupling. Effectively, this would amount to a form of reservoir engineering.

State preparation & cooling Another, more modest application of Lindblad simulation is state preparation, and in particular, cooling. One could imagine preparing a desired system state ρ_S by engineering an effective Liouvillian \mathcal{L}_{eff} which has ρ_S as a unique steady state. [If $\ker(\mathcal{L}_{\text{eff}})$ is 1-dimensional and includes ρ_S , then evolution by $e^{\mathcal{L}_{\text{eff}}t}$ will drive any initial system state towards ρ_S .]

If ρ_S is a thermal state, this dissipative state preparation amounts to cooling. More precisely, it is effectively heat bath algorithmic cooling [12] (HBAC), albeit formulated in an analogue way, and with weak “entropy compression” steps performed at an unusually high rate. We note that the achievable purity of ρ_S through HBAC is known for a given ρ_A [85, 84]. Presumably, the steady states of \mathcal{L}_{eff} , as a function of ρ_A or $\{\rho_A^{(j)}\}$ should also be subject to this bound. Therefore, we expect that results from algorithmic cooling should provide insight into the family of effective Liouvillians that can be simulated using this extended scheme.

More precise coherent control Finally, the higher-order effects analysed in this chapter could be used simply to refine the coherent control scheme from Chapter 4. For instance, the Hamiltonian part of the system’s effective dynamics has terms that go as $\mathcal{O}(\delta t)$; in other words, the truncation error discussed in Section 4.4.1 has both coherent and incoherent components. One could achieve more precise coherent control of S by choosing a sequence $\{\rho_A^{(j)}\}$ which takes into account not only H_{eff} at order $\mathcal{O}(1)$, but also higher-order corrections to the system’s effective Hamiltonians, instead of simply treating these as errors. Finally, one could imagine combining this strategy with the decoupling discussed above to both rapidly control S and extend its coherence times.

Finally, we note that while the results in Chapters 4 and 5 concern the evolution of quantum states, they could easily be adapted to describe the evolution of superoperators (such as quantum channels) by applying Chernoff’s theorem to maps on the set of superoperators.

Chapter 6

Conclusions

In this thesis we examined the problem of indirect quantum control: that of steering a quantum system via a quantum actuator. To do so, we considered the model of a repeated interaction system (RIS), in which a quantum system is coupled to an ancilla for a fixed period of time, after which the ancilla is either reinitialized, or discarded and replaced with a fresh ancilla. We introduced the formalism associated with this model through a preliminary application: describing the quantum Zeno effect (QZE) in realistic settings. Interpreting the RIS ancillas as measurement devices, we showed that the conventional QZE was a special instance of a more general Zeno-like effect, in which a system's state could be preserved through measurements which could be imperfect and repeated at a finite frequency.

We then expanded upon this preliminary result to describe not only state preservation but general coherent control. Interpreting the ancilla as a quantum actuator rather than a measurement device, we showed how one could indirectly control a quantum system by resetting, or more generally, reinitializing, the actuator at a high rate. Concretely, we found that to leading order in the inverse actuator reinitialization frequency, the system's Hamiltonian became non-trivially modified, while the dissipative part of its dynamics did not. This could, in principle, help to improve the ratio of control timescales (e.g., gate times) to coherence times when steering quantum systems. Moreover, our scheme maps the potentially difficult problem of indirect quantum control to the simpler one of direct control. Crucially, it does so for (almost) any system and actuator, with only very weak requirements on the coupling between the two.

We discussed the prospect of extending this indirect control scheme to allow not only coherent, but also dissipative indirect control of a system. We introduced a number of

technical tools to this effect, and discussed several potential applications, including state preparation and cooling, decoupling of the system from its environment, and Lindblad simulation.

Perhaps the main appeal of the indirect control scheme presented here is its immediate applicability to nearly any system-actuator pair. While it may not generally outperform device-dependent schemes which exploit specific properties of certain system-actuator Hamiltonians, our one-size-fits-all approach could be immediately applicable to new system-actuator combinations, as soon as they are realized experimentally. This feature is particularly appealing given the growing interest in hybrid quantum systems [107].

Finally, while the phenomenon of a system's Hamiltonian becoming modified by rapid interactions with a succession of ancillas has been viewed here as a potential tool for realizing quantum technologies, it may also play a role in more fundamental physics. For instance, the Hamiltonian of a quantum system could become effectively modified if the system is constantly bombarded by external particles (such as cosmic rays, neutrinos, dark matter etc.). This effect might be used to detect such incident particles. Similarly, one might expect that a quantum system moving sufficiently rapidly through a quantum field could have its Hamiltonian modified, as the field at different points in space could serve as ancillas with which the system briefly interacts. Finally, one could perhaps imagine seemingly disjoint aspects of a physical theory (say, different sectors of the Standard Model) as emerging, analogously to H_{eff} , due to interactions with an unseen ancillary object or field.

APPENDICES

Appendix A

Eigenpairs of the channel Φ

In the general case of finite frequency measurements, certain eigenpairs of Φ are highly involved functions of the measurement parameters δt_F , δt_M , ω , and g . In the main text, we gave explicit expressions for two particularly simple eigenvalues, and restricted ourselves to a more qualitative discussion of the other eigenvalues and eigenvectors.

Here, we provide a matrix representation for Φ , from which the eigenpairs can easily be extracted using any computer algebra system. The rationale is that the expressions for certain eigenpairs have on the order of 1000 terms, and are thus too lengthy to be useful when written out explicitly. In particular, we define a 4×4 matrix M^Φ , such that if $A = \Phi(B)$, where A and B are matrices on the system's Hilbert space, then

$$\text{vec}(A) = M^\Phi \text{vec}(B), \tag{A.1}$$

where the vectorization operation¹ is defined as

$$\text{vec} \begin{pmatrix} a_{1,1} & a_{1,2} \\ a_{2,1} & a_{2,2} \end{pmatrix} \equiv \begin{pmatrix} a_{1,1} \\ a_{2,1} \\ a_{1,2} \\ a_{2,2} \end{pmatrix}. \tag{A.2}$$

The eigenvalues of Φ are the same as those of M^Φ . The eigenvectors of Φ can be determined by inverting the vectorization operation on those of the M^Φ . The nonzero elements of M^Φ are as follows:

¹This is only one particular choice of an isomorphism—other maps will also work, see, e.g., Section 5.3.1.

$$M_{11}^{\Phi} = \frac{2[(g^3\Omega + g^4 + 2g^2\omega^2)\cos^2(\Omega\delta t_M) + 4\Omega g\omega^2 + 4g^2\omega^2 + 8\omega^4]}{\Omega^2(g + \Omega)^2}, \quad (\text{A.3})$$

$$M_{1,4}^{\Phi} = \frac{(\Omega g + g^2 + 4\omega^2)^2 \sin^2(\Omega\delta t_M)}{\Omega^2(g + \Omega)^2}, \quad (\text{A.4})$$

$$M_{2,2}^{\Phi} = \overline{M_{3,3}^{\Phi}} = \left\{ \cos(g\delta t_M)(\Omega g + \Omega^2)e^{2i\omega\delta t_f} [(\Omega g + g^2 + 4\omega^2)\cos(\Omega\delta t_M) \right. \quad (\text{A.5})$$

$$\left. + 2i(\omega\Omega + 2\omega g)\sin(\Omega\delta t_M) \right\} / [\Omega^2(g + \Omega)^2], \quad (\text{A.6})$$

$$M_{2,3}^{\Phi} = \overline{M_{3,2}^{\Phi}} = \frac{e^{-2i\omega\delta t_f} g \sin(\Omega\delta t_M) \sin(g\delta t_M)(\Omega g + g^2 + 4\omega^2)}{\Omega^2(g + \Omega)^2}, \quad (\text{A.7})$$

$$M_{4,1}^{\Phi} = \frac{g^2 \sin^2(\Omega\delta t_M)}{\Omega^2}, \quad (\text{A.8})$$

$$M_{4,4}^{\Phi} = \frac{(\Omega g + g^2 + 4\omega^2)^2 \cos^2(\Omega\delta t_M)}{\Omega^2(g + \Omega)^2}, \quad (\text{A.9})$$

where $\Omega = \sqrt{g^2 + 4\omega^2}$.

Appendix B

Applying Chernoff's Theorem

In this appendix we verify that Chernoff's theorem can be applied to the map Φ defined in Eq. (4.7). We begin with some definitions, where \mathcal{H} is a separable complex Hilbert space.

Definition. Let $L(\mathcal{H})$ denote the set of linear operators on \mathcal{H} , and let $B(\mathcal{H}) \subset L(\mathcal{H})$ denote the subset of linear operators on \mathcal{H} which are bounded with respect to the operator norm induced by the inner product on \mathcal{H} .

Definition. $X \in B(\mathcal{H})$ is said to be in the trace class if

$$\sum_j \langle \sqrt{X^\dagger X} \phi_j, \phi_j \rangle < \infty \quad (\text{B.1})$$

for all orthonormal sequences $\{\phi_j\}_j \subset \mathcal{H}$ [44], where $\langle \cdot, \cdot \rangle$ denotes the inner product on \mathcal{H} . Let $T(\mathcal{H}) \subset B(\mathcal{H}) \subset L(\mathcal{H})$ denote the set of self-adjoint trace-class elements of $B(\mathcal{H})$. If \mathcal{H} is the state space of a quantum system, then all possible density operators for the system form a subset of $T(\mathcal{H})$.

Definition. We define the function $\|\cdot\|_{\text{tr}}^{\mathcal{H}} : T(\mathcal{H}) \rightarrow \mathbb{R}_{\geq 0}$ by

$$\|X\|_{\text{tr}}^{\mathcal{H}} = \text{tr} \sqrt{X^\dagger X} \quad \forall X \in T(\mathcal{H}). \quad (\text{B.2})$$

It is well-known that $\|\cdot\|_{\text{tr}}^{\mathcal{H}}$ is defined everywhere on $T(\mathcal{H})$, that it constitutes a norm (called the trace norm) on the latter, and that the pair $(T(\mathcal{H}), \|\cdot\|_{\text{tr}}^{\mathcal{H}})$ forms a real Banach space [96].

Definition. Let \mathcal{H}' be a complex separable Hilbert space. We will denote as $\mathfrak{L}(\mathcal{H}, \mathcal{H}')$ the set of linear maps from $T(\mathcal{H})$ to $L(\mathcal{H}')$. When $\mathcal{H} = \mathcal{H}'$ we will simply write $\mathfrak{L}(\mathcal{H})$.

Definition. Let $\|\cdot\|_{\mathfrak{L}(\mathcal{H}, \mathcal{H}')}$ denote the operator norm on $\mathfrak{L}(\mathcal{H}, \mathcal{H}')$. Concretely, for $f \in \mathfrak{L}(\mathcal{H}, \mathcal{H}')$, if there exists a $k \geq 0$ such that $\|f(X)\|_{\text{tr}}^{\mathcal{H}' } \leq k\|X\|_{\text{tr}}^{\mathcal{H}}$ for all $X \in T(\mathcal{H})$ then

$$\|f\|_{\mathfrak{L}(\mathcal{H}, \mathcal{H}')} = \max_{X \in S(\mathcal{H})} \|f(X)\|_{\text{tr}}^{\mathcal{H}' }, \quad (\text{B.3})$$

where $S(\mathcal{H}) = \{X \in T(\mathcal{H}) : \|X\|_{\text{tr}}^{\mathcal{H}} = 1\}$ is the unit sphere in $T(\mathcal{H})$. We take a maximum instead of a supremum in Eq. (B.3) because $S(\mathcal{H})$ (as a closed subset of $T(\mathcal{H})$, a compact set [58]) is compact, and therefore $\|f(X)\|_{\text{tr}}^{\mathcal{H}' }$ attains its supremum on this set.

Definition. Let $\mathfrak{B}(\mathcal{H}, \mathcal{H}') \subset \mathfrak{L}(\mathcal{H}, \mathcal{H}')$ denote the subset of linear maps from $T(\mathcal{H})$ to $L(\mathcal{H}')$ that are bounded with respect to $\|\cdot\|_{\mathfrak{L}(\mathcal{H}, \mathcal{H}')}$. When $\mathcal{H} = \mathcal{H}'$ we write $\mathfrak{B}(\mathcal{H})$.

Let us now verify that Φ satisfies the conditions for Chernoff's theorem.

Theorem (Chernoff's theorem). Let $F(\delta t)$, $0 \leq \delta t < \infty$ be an operator-valued function on a Banach space $(B, \|\cdot\|)$. If

1. $F(\delta t)$ is strongly continuous with respect to δt ,
2. $F(\delta t)$ is a linear operator on B , and $\|F(\delta t)\|_O \leq 1$ for all $\delta t \geq 0$, where $\|\cdot\|_O$ denotes the operator norm induced by $\|\cdot\|$;
3. $F(0) = \text{id}_B$,
4. The strong derivative $F'(0)$ exists, and its closure C is the generator of a semigroup,

then $\lim_{n \rightarrow \infty} F(t/n)^n = e^{Ct}$ in the strong operator topology.

We proceed to verify conditions 1-4 for $\Phi(\delta t)$. We will identify the Banach space in the theorem statement $(B, \|\cdot\|)$ with $(T(\mathcal{H}_S), \|\cdot\|_{\text{tr}}^{\mathcal{H}_S})$, the Banach space of trace-class self-adjoint linear operators on \mathcal{H}_S , the system's Hilbert space. We will also identify the function F with Φ .

B.1 Continuity of $\Phi(\delta t)$

Let us write Φ as the composition of two functions. Define $\mathcal{V} : \mathbb{R}_{\geq 0} \rightarrow \mathfrak{B}(\mathcal{H}_S, \mathcal{H}_S \otimes \mathcal{H}_A)$, where \mathcal{H}_A is the actuator's Hilbert space, as

$$\mathcal{V}(\delta t)X = \mathcal{T} \exp \left[\int_0^{\delta t} d\tau \mathcal{L}(\tau) \right] (X \otimes \rho_A) \quad (\text{B.4})$$

for all $X \in T(\mathcal{H}_S)$ and $\delta t \in \mathbb{R}_{\geq 0}$. Let $\mathcal{P} : \mathfrak{B}(\mathcal{H}_S, \mathcal{H}_S \otimes \mathcal{H}_A) \rightarrow \mathfrak{B}(\mathcal{H}_S)$ be defined as

$$(\mathcal{P}f)(\cdot) = \text{tr}_A [f(\cdot)] \quad (\text{B.5})$$

for any $f \in \mathfrak{B}(\mathcal{H}_S, \mathcal{H}_S \otimes \mathcal{H}_A)$. We have that $\Phi = \mathcal{P} \circ \mathcal{V}$. Let us now show that both \mathcal{P} and \mathcal{V} are continuous functions, from which it follows that Φ is continuous as well.

Continuity of \mathcal{V} is clear, as this function describes evolution by the Lindblad equation with the initial condition $\mathcal{V}(0)X = X \otimes \rho_A$. Nevertheless, let us sketch an argument for its continuity. Following the derivation in Section 4.2, we have that

$$V(\delta t)X = X \otimes \rho_A + \sum_{k=1}^{\infty} \int_0^{\delta t} d\tau_1 \int_0^{\tau_1} d\tau_2 \cdots \int_0^{\tau_{k-1}} d\tau_k \mathcal{L}(\tau_1)\mathcal{L}(\tau_2) \cdots \mathcal{L}(\tau_k) X \otimes \rho_A. \quad (\text{B.6})$$

Taking $t, c \geq 0$, we have

$$V(t)X - V(c)X = \sum_{k=1}^{\infty} \int_c^t d\tau_1 \int_0^{\tau_1} d\tau_2 \cdots \int_0^{\tau_{k-1}} d\tau_k \mathcal{L}(\tau_1)\mathcal{L}(\tau_2) \cdots \mathcal{L}(\tau_k) X \otimes \rho_A, \quad (\text{B.7})$$

therefore $\|V(t) - V(c)\|_{\mathfrak{L}(\mathcal{H}_S \otimes \mathcal{H}_A)} \rightarrow 0$ as $|t - c| \rightarrow 0$.

We now consider \mathcal{P} . Since the partial trace is a completely positive trace-preserving (CPTP) map [41], it is contractive under the trace norm (see Section B.2) [80]. For any $X \in T(\mathcal{H}_S)$ and $f \in \mathfrak{B}(\mathcal{H}_S, \mathcal{H}_S \otimes \mathcal{H}_A)$, define $Y = f(X)$. We have

$$\|(\mathcal{P}f)(X)\|_{\text{tr}}^{\mathcal{H}_S} = \|\text{tr}_A Y\|_{\text{tr}}^{\mathcal{H}_S} \leq \|Y\|_{\text{tr}}^{\mathcal{H}_S \otimes \mathcal{H}_A} = \|f(X)\|_{\text{tr}}^{\mathcal{H}_S \otimes \mathcal{H}_A}. \quad (\text{B.8})$$

Maximizing both sides of (B.8) over $X \in S(\mathcal{H}_S)$, we find that

$$\|\mathcal{P}f\|_{\mathfrak{L}(\mathcal{H}_S)} \leq \|f\|_{\mathfrak{L}(\mathcal{H}_S, \mathcal{H}_S \otimes \mathcal{H}_A)}. \quad (\text{B.9})$$

In other words, \mathcal{P} is bounded (contractive, even). Moreover, since it also a linear map, \mathcal{P} is continuous [61]. Therefore, $\Phi = \mathcal{P} \circ \mathcal{V}$ is continuous as well.

B.2 Linearity and contractivity of $\Phi(\delta t)$

Linearity is clear from Eq. (4.7). For any $\delta t \geq 0$, $\Phi(\delta t)$ is a CPTP map, and it is well known that such maps are contractive with respect to the trace norm [80]. Nevertheless,

we will sketch a proof of this result. Any $X \in T(\mathcal{H}_S)$ admits a spectral decomposition of the form

$$X = \int_{\text{spec}(X)} \lambda dP(\lambda), \quad (\text{B.10})$$

where $P(\lambda)$ is an appropriate projection-valued measure [42]. One can define positive and negative components of X , which we denote X_+ and X_- respectively, as

$$X_{\pm} = \int_{\text{spec}(X) \cap \mathbb{R}_{\pm}} \lambda dP(\lambda). \quad (\text{B.11})$$

Notice that $X_+ > 0$, $X_- < 0$, and that $X = X_+ + X_-$. Furthermore

$$\begin{aligned} \|X\|_{\text{tr}}^{\mathcal{H}_S} &= \text{tr} |X| = \text{tr}(X_+) + \text{tr}(-X_-) \\ &= \text{tr} |X_+| + \text{tr} |X_-| = \|X_+\|_{\text{tr}}^{\mathcal{H}_S} + \|X_-\|_{\text{tr}}^{\mathcal{H}_S}. \end{aligned} \quad (\text{B.12})$$

Using this result, we have that for $f \in \mathfrak{B}(\mathcal{H}_S)$

$$\begin{aligned} \|f(X)\|_{\text{tr}}^{\mathcal{H}_S} &= \|f(X_+) + f(X_-)\|_{\text{tr}}^{\mathcal{H}_S} \\ &\leq \|f(X_+)\|_{\text{tr}}^{\mathcal{H}_S} + \|f(-X_-)\|_{\text{tr}}^{\mathcal{H}_S} \\ &= \|X_+\|_{\text{tr}}^{\mathcal{H}_S} + \|-X_-\|_{\text{tr}}^{\mathcal{H}_S} \\ &= \|X\|_{\text{tr}}^{\mathcal{H}_S}. \end{aligned} \quad (\text{B.13})$$

Therefore, $\Phi(\delta t)$ is a linear contraction with respect to $\|\cdot\|_{\mathfrak{L}(\mathcal{H}_S)}$ for all $\delta t \geq 0$.

B.3 $\Phi(0)$ is the identity operator on B

$$\Phi(0)X = \text{tr}_A(X \otimes \rho_A) = X \implies \Phi(0) = \text{id}_{T(\mathcal{H}_S)}. \quad (\text{B.14})$$

B.4 Existence of $\Phi'(0)$ and semigroup property

The strong derivative $\Phi'(0)$ refers to the operator

$$\Phi'(0)X = \lim_{\delta t \rightarrow 0} \frac{\Phi(\delta t)X - X}{\delta t}, \quad (\text{B.15})$$

defined for all $X \in T(\mathcal{H}_S)$ for which the limit exists [27]. From the series $\Phi(\delta t) = I + \delta t \Phi_1 + \delta t^2 \Phi_2 + \dots$ we see that $\Phi'(0) = \Phi_1$. Moreover, it is apparent from Eqs. (4.14) and (4.19) that Φ_1 is a Liouvillian, and therefore, the generator of a semigroup [7]. It follows that to leading order in $1/n$, the system evolves according to

$$\rho_S(t) = e^{Ct} \rho_S(0), \quad (\text{B.16})$$

where C is the closure of Φ_1 . However, for the purposes of studying the system's physical evolution, it suffices to consider $\rho_S \in \text{dom}(\Phi_1)$. Since $C \upharpoonright_{\text{dom}(\Phi_1)} = \Phi_1$, we can apply Chernoff's theorem to find

$$\rho_S(t) = e^{\Phi_1 t} \rho_S(0), \quad (\text{B.17})$$

or equivalently

$$i\hbar \frac{\partial}{\partial t} \rho_S(t) = [H_{\text{eff}}, \rho_S(t)] \quad (\text{B.18})$$

for all physical states of the system $\rho_S(t)$, as $n \rightarrow \infty$.

Appendix C

Simulation Details

The simulation described in Section 4.3.3 was performed using QuTiP [54]. The Hilbert space of the harmonic oscillator was truncated to a 25-dimensional space spanned by the Fock states $|0\rangle, \dots, |24\rangle$. We will denote by $\tilde{\mathcal{H}}_S = \text{span}\{|n\rangle\}_{n=0}^{24}$ this truncated space. Creation and annihilation operators were defined on $\tilde{\mathcal{H}}_S$ by their action on Fock states:

$$\tilde{a}|n\rangle = \begin{cases} \sqrt{n}|n-1\rangle & 1 \leq n \leq 24 \\ 0 & n = 0 \end{cases} \quad (\text{C.1})$$

$$\tilde{a}^\dagger|n\rangle = \begin{cases} \sqrt{n+1}|n+1\rangle & 0 \leq n \leq 23 \\ 0 & n = 24. \end{cases} \quad (\text{C.2})$$

The number and position operators on $\tilde{\mathcal{H}}_S$ were defined as $\tilde{N} = \tilde{a}^\dagger\tilde{a}$ and $\tilde{X} = (\tilde{a}^\dagger + \tilde{a})/2$ respectively.

The dimension of $\tilde{\mathcal{H}}_S$ required to accurately simulate the full oscillator was determined by producing versions of Fig. 4.3 for truncated oscillator Hilbert spaces of different dimensions d , and comparing the resulting curves. (This was done for actuator reset frequencies $f = 2\nu, 5\nu$, and 10ν .) In particular, Fig. C.1 shows the average distance between the $F(t)$ curves resulting from $\dim(\tilde{\mathcal{H}}_S) = d$ and $\dim(\tilde{\mathcal{H}}_S) = d - 1$. Notice that this distance is vanishingly small past $d = 15$. In other words, the harmonic oscillator's state did not take on any appreciable components with an excitation number greater than 15 over the course of our simulation. Nevertheless, in order to be cautious, we produced Fig. 4.3 using $d = 25$.

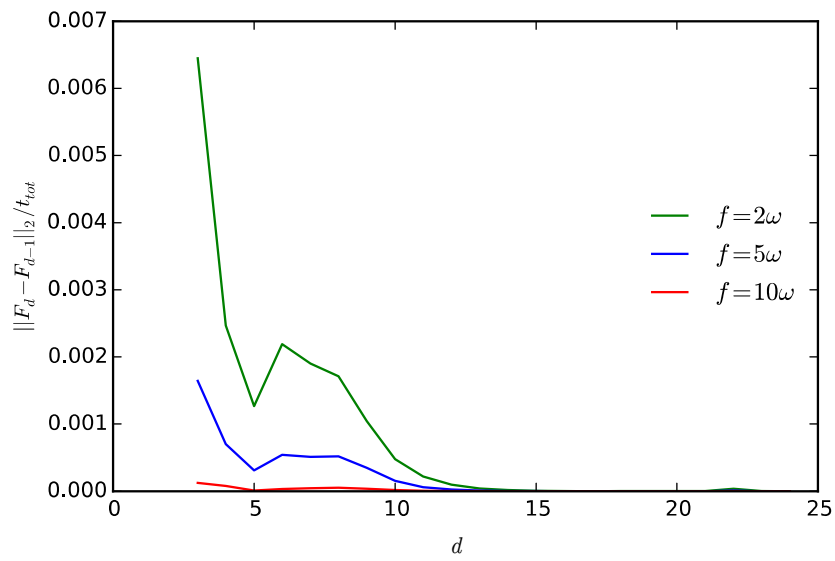


Figure C.1: Shown is the average root-mean-squared distance between $F(t)$ curves, of the type shown in Fig. 4.3, corresponding to successive values of $d = \dim(\tilde{\mathcal{H}}_S)$. The parameters used are listed in the caption of Fig. 4.3. Notice that increasing d beyond $d \approx 15$ produced little change in the resulting $F(t)$ curves for all three values of f considered. This figure was made using QuTiP [54].

References

- [1] Clarice D. Aiello and Paola Cappellaro. Time-optimal control by a quantum actuator. *Phys. Rev. A*, 91:042340, Apr 2015.
- [2] Victor V Albert, Barry Bradlyn, Martin Fraas, and Liang Jiang. Geometry and response of lindbladians. *arXiv:1512.08079*, 2015.
- [3] Mario Argeri, Stefano Di Vita, Pierpaolo Mastrolia, Edoardo Mirabella, Johannes Schlenk, Ulrich Schubert, and Lorenzo Tancredi. Magnus and dyson series for master integrals. *J. High Energy Phys*, 2014(3):1–32, 2014.
- [4] Stéphane Attal and Alain Joye. The langevin equation for a quantum heat bath. *J. Funct. Anal.*, 247(2):253 – 288, 2007.
- [5] Stéphane Attal and Alain Joye. Weak coupling and continuous limits for repeated quantum interactions. *J. Stat. Phys*, 126(6):1241–1283, 2007.
- [6] Stéphane Attal and Yan Pautrat. From repeated to continuous quantum interactions. *Ann. Henri Poincaré*, 7(1):59–104, 2006.
- [7] A. Barchielli and M. Gregoratti. *Quantum Trajectories and Measurements in Continuous Time: The Diffusive Case*. Lecture Notes in Physics. Springer Berlin Heidelberg, 2009.
- [8] R. Barends, J. Kelly, A. Megrant, A. Veitia, D. Sank, E. Jeffrey, T. C. White, J. Mutus, A. G. Fowler, B. Campbell, Y. Chen, Z. Chen, B. Chiaro, A. Dunsworth, C. Neill, P. O’Malley, P. Roushan, A. Vainsencher, J. Wenner, A. N. Korotkov, A. N. Cleland, and J. M. Martinis. Superconducting quantum circuits at the surface code threshold for fault tolerance. *Nature*, 508(7497):500–503, 2014.

- [9] Almut Beige, Daniel Braun, Ben Tregenna, and Peter L. Knight. Quantum computing using dissipation to remain in a decoherence-free subspace. *Phys. Rev. Lett.*, 85:1762–1765, Aug 2000.
- [10] V. Bentkus. A new method for approximations in probability and operator theories. *Lithuanian Math. J.*, 43(4):367–388, 2003.
- [11] Michael J Biercuk, Hermann Uys, Aaron P VanDevender, Nobuyasu Shiga, Wayne M Itano, and John J Bollinger. Optimized dynamical decoupling in a model quantum memory. *Nature*, 458(7241):996–1000, 2009.
- [12] P. Oscar Boykin, Tal Mor, Vwani Roychowdhury, Farrokh Vatan, and Rutger Vrijen. Algorithmic cooling and scalable nmr quantum computers. *Proc. Natl. Acad. Sci.*, 99(6):3388–3393, 2002.
- [13] H.P. Breuer and F. Petruccione. *The Theory of Open Quantum Systems*. Oxford University Press, 2002.
- [14] Wesley E. Brittin and Walter Wyss. Taylor’s theorem for analytic functions of operators. *Commun. Math. Phys.*, 49(2):107–112, 1976.
- [15] R. Bronson. *Matrix Methods: An Introduction*. Academic Press, 1991.
- [16] L.E.J. Brouwer. ber abbildung von mannigfaltigkeiten. *Math. Ann.*, 71(1):97–115, 1911.
- [17] L. Bruneau and C.-A. Pillet. Thermal relaxation of a qed cavity. *J. Stat. Phys.*, 134(5):1071–1095, 2008.
- [18] Laurent Bruneau. Mixing properties of the one-atom maser. *J. Stat. Phys.*, 155(5):888–908, 2014.
- [19] Laurent Bruneau, Alain Joye, and Marco Merkli. Asymptotics of repeated interaction quantum systems. *J. Funct. Anal.*, 239(1):310–344, 2006.
- [20] Laurent Bruneau, Alain Joye, and Marco Merkli. Random repeated interaction quantum systems. *Commun. Math. Phys.*, 284(2):553–581, 2008.
- [21] Laurent Bruneau, Alain Joye, and Marco Merkli. Repeated interactions in open quantum systems. *J. Math. Phys.*, 55(7), 2014.

- [22] Daniel Burgarth, Sougato Bose, Christoph Bruder, and Vittorio Giovannetti. Local controllability of quantum networks. *Phys. Rev. A*, 79:060305, Jun 2009.
- [23] Daniel Burgarth, Koji Maruyama, Michael Murphy, Simone Montangero, Tommaso Calarco, Franco Nori, and Martin B. Plenio. Scalable quantum computation via local control of only two qubits. *Phys. Rev. A*, 81:040303, Apr 2010.
- [24] P. Cappellaro, L. Jiang, J. S. Hodges, and M. D. Lukin. Coherence and control of quantum registers based on electronic spin in a nuclear spin bath. *Phys. Rev. Lett.*, 102:210502, May 2009.
- [25] Mo Chen, Masashi Hirose, and Paola Cappellaro. Measurement of transverse hyperfine interaction by forbidden transitions. *Phys. Rev. B*, 92:020101, Jul 2015.
- [26] Paul R. Chernoff. Note on product formulas for operator semigroups. *J. Funct. Anal.*, 2(2):238 – 242, 1968.
- [27] Paul R. Chernoff. Semigroup product formulas and addition of unbounded operators. *Bull. Amer. Math. Soc.*, 76(2):395–398, 03 1970.
- [28] Paul R. Chernoff. On the converse of the trotter product formula. *Illinois J. Math.*, 20(2):348–353, 06 1976.
- [29] P. C. De Groot, J. Lisenfeld, R. N. Schouten, S. Ashhab, A. Lupuşcu, C. J. P. M. Harman, and J. E. Mooij. Selective darkening of degenerate transitions demonstrated with two superconducting quantum bits. *Nat. Phys.*, 6(10):763–766, 2010.
- [30] Jason M Dominy, Gerardo A Paz-Silva, A T Rezakhani, and D A Lidar. Analysis of the quantum zeno effect for quantum control and computation. *J. Phys. A*, 46(7):075306, 2013.
- [31] Noam Erez, Yakir Aharonov, Benni Reznik, and Lev Vaidman. Correcting quantum errors with the zeno effect. *Phys. Rev. A*, 69:062315, Jun 2004.
- [32] P. Facchi, V. Gorini, G. Marmo, S. Pascazio, and E.C.G. Sudarshan. Quantum zeno dynamics. *Phys. Lett. A*, 275(12):12 – 19, 2000.
- [33] Z. Ficek and M.R. Wahiddin. *Quantum Optics for Beginners*. Pan Stanford, Singapore, 2014.

- [34] M. C. Fischer, B. Gutiérrez-Medina, and M. G. Raizen. Observation of the quantum zeno and anti-zeno effects in an unstable system. *Phys. Rev. Lett.*, 87:040402, Jul 2001.
- [35] J. D. Franson, B. C. Jacobs, and T. B. Pittman. Quantum computing using single photons and the zeno effect. *Phys. Rev. A*, 70:062302, Dec 2004.
- [36] Jay Gambetta, Alexandre Blais, D. I. Schuster, A. Wallraff, L. Frunzio, J. Majer, M. H. Devoret, S. M. Girvin, and R. J. Schoelkopf. Qubit-photon interactions in a cavity: Measurement-induced dephasing and number splitting. *Phys. Rev. A*, 74:042318, Oct 2006.
- [37] F.R. Gantmacher. *The Theory of Matrices*. Chelsea Publishing Series. Chelsea, 1959.
- [38] C. Gardiner and P. Zoller. *Quantum Noise: A Handbook of Markovian and Non-Markovian Quantum Stochastic Methods with Applications to Quantum Optics*. Springer Series in Synergetics. Springer, 2004.
- [39] Vittorio Giovannetti and G Massimo Palma. Master equations for correlated quantum channels. *Phys. Rev. Lett.*, 108(4):040401, 2012.
- [40] Daniel Grimmer, David Layden, Eduardo Martin-Martinez, and Robert B Mann. Open dynamics under rapid repeated interaction. *arXiv:1605.04302*, 2016.
- [41] V.P. Gupta, P. Mandayam, and V.S. Sunder. *The Functional Analysis of Quantum Information Theory: A Collection of Notes Based on Lectures by Gilles Pisier, K. R. Parthasarathy, Vern Paulsen and Andreas Winter*. Lecture Notes in Physics. Springer International Publishing, 2015.
- [42] B.C. Hall. *Quantum Theory for Mathematicians*. Graduate Texts in Mathematics. Springer, 2013.
- [43] Eric Hanson, Alain Joye, Yan Pautrat, and Renaud Raquépas. Landauer’s principle in repeated interaction systems. *arXiv:1510.00533*, 2015.
- [44] T. Heinosaari and M. Ziman. *The Mathematical Language of Quantum Theory: From Uncertainty to Entanglement*. Cambridge University Press, 2011.
- [45] Rahel Heule, C. Bruder, Daniel Burgarth, and Vladimir M. Stojanović. Local quantum control of heisenberg spin chains. *Phys. Rev. A*, 82:052333, Nov 2010.

- [46] M Hirose and P Cappellaro. Time-optimal control with finite bandwidth. *arXiv:1510.06801*, 2015.
- [47] J. S. Hodges, J. C. Yang, C. Ramanathan, and D. G. Cory. Universal control of nuclear spins via anisotropic hyperfine interactions. *Phys. Rev. A*, 78:010303, Jul 2008.
- [48] A.S. Holevo. *Quantum Systems, Channels, Information: A Mathematical Introduction*. De Gruyter Studies in Mathematical Physics. De Gruyter, 2013.
- [49] D Hucul, IV Inlek, G Vittorini, C Crocker, S Debnath, SM Clark, and CI Monroe. Modular entanglement of atomic qubits using photons and phonons. *Nature Physics*, 11(1):37–42, 2015.
- [50] E. K. Irish and K. Schwab. Quantum measurement of a coupled nanomechanical resonator-cooper-pair box system. *Phys. Rev. B*, 68:155311, Oct 2003.
- [51] Wayne M. Itano, D. J. Heinzen, J. J. Bollinger, and D. J. Wineland. Quantum zeno effect. *Phys. Rev. A*, 41:2295–2300, Mar 1990.
- [52] Kurt Jacobs. Engineering quantum states of a nanoresonator via a simple auxiliary system. *Phys. Rev. Lett.*, 99:117203, Sep 2007.
- [53] Evan Jeffrey, Daniel Sank, J. Y. Mutus, T. C. White, J. Kelly, R. Barends, Y. Chen, Z. Chen, B. Chiaro, A. Dunsworth, A. Megrant, P. J. J. O’Malley, C. Neill, P. Roushan, A. Vainsencher, J. Wenner, A. N. Cleland, and John M. Martinis. Fast accurate state measurement with superconducting qubits. *Phys. Rev. Lett.*, 112:190504, May 2014.
- [54] J.R. Johansson, P.D. Nation, and Franco Nori. Qutip 2: A python framework for the dynamics of open quantum systems. *Comput. Phys. Commun.*, 184(4):1234 – 1240, 2013.
- [55] Dragi Karevski and Thierry Platini. Quantum nonequilibrium steady states induced by repeated interactions. *Phys. Rev. Lett.*, 102(20):207207, 2009.
- [56] J. Kempe, D. Bacon, D. A. Lidar, and K. B. Whaley. Theory of decoherence-free fault-tolerant universal quantum computation. *Phys. Rev. A*, 63:042307, Mar 2001.
- [57] Navin Khaneja, Timo Reiss, Cindie Kehlet, Thomas Schulte-Herbruggen, and Stefan J. Glaser. Optimal control of coupled spin dynamics: design of {NMR} pulse sequences by gradient ascent algorithms. *J. Magn. Reson.*, 172(2):296 – 305, 2005.

- [58] A.W. Knap. *Advanced Real Analysis*. Cornerstones. Birkhäuser Boston, 2008.
- [59] Emanuel Knill, Raymond Laflamme, and Wojciech H Zurek. Resilient quantum computation. *Science*, 279(5349):342–345, 1998.
- [60] AG Kofman and G Kurizki. Acceleration of quantum decay processes by frequent observations. *Nature*, 405(6786):546–550, 2000.
- [61] E. Kreyszig. *Introductory Functional Analysis with Applications*.
- [62] Paul G Kwiat, Andrew J Berglund, Joseph B Altepeter, and Andrew G White. Experimental verification of decoherence-free subspaces. *Science*, 290(5491):498–501, 2000.
- [63] MD LaHaye, J Suh, PM Echternach, KC Schwab, and ML Roukes. Nanomechanical measurements of a superconducting qubit. *Nature*, 459(7249):960–964, 2009.
- [64] David Layden, Eduardo Martín-Martínez, and Achim Kempf. Perfect zeno-like effect through imperfect measurements at a finite frequency. *Phys. Rev. A*, 91:022106, Feb 2015.
- [65] David Layden, Eduardo Martín-Martínez, and Achim Kempf. Universal scheme for indirect quantum control. *Phys. Rev. A*, 93:040301, Apr 2016.
- [66] D. A. Lidar, I. L. Chuang, and K. B. Whaley. Decoherence-free subspaces for quantum computation. *Phys. Rev. Lett.*, 81:2594–2597, Sep 1998.
- [67] D.A. Lidar and T.A. Brun. *Quantum Error Correction*. Cambridge University Press, 2013.
- [68] Goran Lindblad. On the generators of quantum dynamical semigroups. *Commun. Math. Phys*, 48(2):119–130, 1976.
- [69] Seth Lloyd. Almost any quantum logic gate is universal. *Phys. Rev. Lett.*, 75:346–349, Jul 1995.
- [70] Seth Lloyd and Samuel L. Braunstein. Quantum computation over continuous variables. *Phys. Rev. Lett.*, 82:1784–1787, Feb 1999.
- [71] Seth Lloyd, Andrew J. Landahl, and Jean-Jacques E. Slotine. Universal quantum interfaces. *Phys. Rev. A*, 69:012305, Jan 2004.

- [72] Seth Lloyd and Lorenza Viola. Engineering quantum dynamics. *Phys. Rev. A*, 65:010101, Dec 2001.
- [73] J Majer, JM Chow, JM Gambetta, Jens Koch, BR Johnson, JA Schreier, L Frunzio, DI Schuster, AA Houck, Andreas Wallraff, A. Blais, M. H. Devoret, S. M. Girvin, and R. J. Schoelkopf. Coupling superconducting qubits via a cavity bus. *Nature*, 449(7161):443–447, 2007.
- [74] Eduardo Martín-Martínez, David Aasen, and Achim Kempf. Processing quantum information with relativistic motion of atoms. *Phys. Rev. Lett.*, 110:160501, Apr 2013.
- [75] Eduardo Martín-Martínez, Eric G. Brown, William Donnelly, and Achim Kempf. Sustainable entanglement production from a quantum field. *Phys. Rev. A*, 88:052310, Nov 2013.
- [76] John JL Morton, Alexei M Tyryshkin, Arzhang Ardavan, Simon C Benjamin, Kyriakos Porfyrikis, SA Lyon, and G Andrew D Briggs. Bang–bang control of fullerene qubits using ultrafast phase gates. *Nature Physics*, 2(1):40–43, 2006.
- [77] John JL Morton, Alexei M Tyryshkin, Richard M Brown, Shyam Shankar, Brendon W Lovett, Arzhang Ardavan, Thomas Schenkel, Eugene E Haller, Joel W Ager, and SA Lyon. Solid-state quantum memory using the 31p nuclear spin. *Nature*, 455(7216):1085–1088, 2008.
- [78] Hiromichi Nakazato, Tomoko Takazawa, and Kazuya Yuasa. Purification through zeno-like measurements. *Phys. Rev. Lett.*, 90:060401, Feb 2003.
- [79] Hiromichi Nakazato, Makoto Unoki, and Kazuya Yuasa. Preparation and entanglement purification of qubits through zeno-like measurements. *Phys. Rev. A*, 70:012303, Jul 2004.
- [80] M.A. Nielsen and I.L. Chuang. *Quantum Computation and Quantum Information*. Cambridge Series on Information and the Natural Sciences. Cambridge University Press, 2000.
- [81] Nissim Ofek, Andrei Petrenko, Reinier Heeres, Philip Reinhold, Zaki Leghtas, Brian Vlastakis, Yehan Liu, Luigi Frunzio, SM Girvin, Liang Jiang, Mazyar Mirrahimi, M. H. Devoret, and R. J. Schoelkopf. Demonstrating quantum error correction that extends the lifetime of quantum information. *arXiv:1602.04768*, 2016.

- [82] Gerardo A. Paz-Silva, A. T. Rezakhani, Jason M. Dominy, and D. A. Lidar. Zeno effect for quantum computation and control. *Phys. Rev. Lett.*, 108:080501, Feb 2012.
- [83] P. Rabl, P. Cappellaro, M. V. Gurudev Dutt, L. Jiang, J. R. Maze, and M. D. Lukin. Strong magnetic coupling between an electronic spin qubit and a mechanical resonator. *Phys. Rev. B*, 79:041302, Jan 2009.
- [84] Sadegh Raeisi and Michele Mosca. Asymptotic bound for heat-bath algorithmic cooling. *Phys. Rev. Lett.*, 114:100404, Mar 2015.
- [85] Nayeli Azucena Rodríguez-Briones and Raymond Laflamme. Achievable polarization for heat-bath algorithmic cooling. *Phys. Rev. Lett.*, 116:170501, Apr 2016.
- [86] Marcelo França Santos. Universal and deterministic manipulation of the quantum state of harmonic oscillators: A route to unitary gates for fock state qubits. *Phys. Rev. Lett.*, 95:010504, Jun 2005.
- [87] Valerio Scarani, Mário Ziman, Peter Štelmachovič, Nicolas Gisin, and Vladimír Bužek. Thermalizing quantum machines: Dissipation and entanglement. *Phys. Rev. Lett.*, 88:097905, Feb 2002.
- [88] J. Schauder. Der fixpunktsatz in funktionalramen. *Stud. Math.*, 2(1):171–180, 1930.
- [89] DI Schuster, AA Houck, JA Schreier, A Wallraff, JM Gambetta, A Blais, L Frunzio, J Majer, B Johnson, MH Devoret, S. M. Girvin, and R. J. Schoelkopf. Resolving photon number states in a superconducting circuit. *Nature*, 445(7127):515–518, 2007.
- [90] M. Shapiro and P. Brumer. *Quantum Control of Molecular Processes*. Wiley, 2012.
- [91] Peter W Shor. Scheme for reducing decoherence in quantum computer memory. *Physical review A*, 52(4):R2493, 1995.
- [92] O.G. Smolyanov, Hv Weizsäcker, and O. Wittich. Brownian motion on a manifold as a limit of stepwise conditioned standard brownian motions. In *Stochastic Processes, Physics, and Geometry: New Interplays*, volume 2 of *Proceedings of the Conference on Infinite Dimensional (Stochastic) Analysis and Quantum Physics*, page 589, 1999.
- [93] O.G. Smolyanov, Hv Weizsäcker, and O. Wittich. Chernoff’s theorem and the construction of semigroups. In *Evolution Equations: Applications to Physics, Industry, Life Sciences and Economics*, volume 55, pages 349–358. Birkhäuser, 2003.

- [94] Andrew Steane. Multiple-particle interference and quantum error correction. *Proc. Roy. Soc. London Ser. A*, 452(1954):2551–2577, 1996.
- [95] Frederick W. Strauch. Quantum logic gates for superconducting resonator qubits. *Phys. Rev. A*, 84:052313, Nov 2011.
- [96] Werner Stulpe. Operator. In Daniel Greenberger, Klaus Hentschel, and Friedel Weinert, editors, *Compendium of Quantum Physics*, pages 440–444. Springer Berlin Heidelberg, 2009.
- [97] Tim Hugo Taminiu, Julia Cramer, Toeno van der Sar, Viatcheslav V Dobrovitski, and Ronald Hanson. Universal control and error correction in multi-qubit spin registers in diamond. *Nature nanotechnology*, 9(3):171–176, 2014.
- [98] William Turin. *Performance Analysis and Modeling of Digital Transmission Systems*. Kluwer Academic/Plenum Publishers, 2004.
- [99] Rodrigo Vargas. Repeated interaction quantum systems: Van hove limits and asymptotic states. *J. Stat. Phys*, 133(3):491–511, 2008.
- [100] Lorenza Viola, Emanuel Knill, and Seth Lloyd. Dynamical decoupling of open quantum systems. *Phys. Rev. Lett.*, 82:2417–2421, Mar 1999.
- [101] Lorenza Viola and Seth Lloyd. Dynamical suppression of decoherence in two-state quantum systems. *Phys. Rev. A*, 58:2733–2744, Oct 1998.
- [102] Lorenza Viola, Seth Lloyd, and Emanuel Knill. Universal control of decoupled quantum systems. *Phys. Rev. Lett.*, 83:4888–4891, Dec 1999.
- [103] K. Vogel, V. M. Akulin, and W. P. Schleich. Quantum state engineering of the radiation field. *Phys. Rev. Lett.*, 71:1816–1819, Sep 1993.
- [104] C. Wang, C. Axline, Y. Y. Gao, T. Brecht, Y. Chu, L. Frunzio, M. H. Devoret, and R. J. Schoelkopf. Surface participation and dielectric loss in superconducting qubits. *Appl. Phys. Lett.*, 107(16), 2015.
- [105] Xiang-Bin Wang, J. Q. You, and Franco Nori. Quantum entanglement via two-qubit quantum zeno dynamics. *Phys. Rev. A*, 77:062339, Jun 2008.
- [106] Michael M Wolf and David Perez-Garcia. The inverse eigenvalue problem for quantum channels. *arXiv:1005.4545*, 2010.

- [107] Ze-Liang Xiang, Sahel Ashhab, J. Q. You, and Franco Nori. Hybrid quantum circuits: Superconducting circuits interacting with other quantum systems. *Rev. Mod. Phys.*, 85:623–653, Apr 2013.
- [108] Paolo Zanardi and Lorenzo Campos Venuti. Coherent quantum dynamics in steady-state manifolds of strongly dissipative systems. *Phys. Rev. Lett.*, 113:240406, Dec 2014.
- [109] Paolo Zanardi and Lorenzo Campos Venuti. Geometry, robustness, and emerging unitarity in dissipation-projected dynamics. *Phys. Rev. A*, 91:052324, May 2015.
- [110] Paolo Zanardi, Jeffrey Marshall, and Lorenzo Campos Venuti. Dissipative universal lindbladian simulation. *Phys. Rev. A*, 93(2):022312, 2016.
- [111] Alessandro Zavatta, Silvia Viciani, and Marco Bellini. Quantum-to-classical transition with single-photon-added coherent states of light. *Science*, 306(5696):660–662, 2004.
- [112] M. Ziman, P. Štelmachovič, V. Bužek, M. Hillery, V. Scarani, and N. Gisin. Diluting quantum information: An analysis of information transfer in system-reservoir interactions. *Phys. Rev. A*, 65:042105, Mar 2002.
- [113] Mário Ziman and Vladimír Bužek. All (qubit) decoherences: Complete characterization and physical implementation. *Phys. Rev. A*, 72:022110, Aug 2005.
- [114] Mário Ziman, Peter Štelmachovič, and Vladimír Bužek. Description of quantum dynamics of open systems based on collision-like models. *Open Syst. Inf. Dyn.*, 12(1):81–91, 2005.
- [115] Wojciech H. Zurek. Decoherence and the transition from quantum to classical. *Physics Today*, 44(10), 1991.
- [116] Wojciech Hubert Zurek. Decoherence, einselection, and the quantum origins of the classical. *Rev. Mod. Phys.*, 75:715–775, May 2003.